J. Fluid Mech. (2003), *vol.* 475, *pp.* 173–203.
DOI: 10.1017/S0022112002002756 Printed in the United Kingdom

Mixed velocity–passive scalar statistics in high-Reynolds-number turbulence

By L. MYDLARSKI

Department of Mechanical Engineering, McGill University,
817 Sherbrooke Street West, Montréal, QC, H3A-2K6, Canada

(Received 30 August 2001 and in revised form 9 August 2002)

Statistics of the mixed velocity–passive scalar field and its Reynolds number dependence are studied in quasi-isotropic decaying grid turbulence with an imposed mean temperature gradient. The turbulent Reynolds number (using the Taylor microscale as the length scale), R_λ, is varied over the range $85 \leqslant R_\lambda \leqslant 582$. The passive scalar under consideration is temperature in air. The turbulence is generated by means of an active grid and the temperature fluctuations result from the action of the turbulence on the mean temperature gradient. The latter is created by differentially heating elements at the entrance to the wind tunnel plenum chamber. The mixed velocity–passive scalar field evolves slowly with Reynolds number. Inertial-range scaling exponents of the co-spectra of transverse velocity and temperature, $E_{v\theta}(k_1)$, and its real-space analogue, the 'heat flux structure function,' $\langle \Delta v(r) \Delta\theta(r) \rangle$, show a slow evolution towards their theoretical predictions of $-7/3$ and $4/3$, respectively. The sixth-order longitudinal mixed structure functions, $\langle (\Delta u(r))^2 (\Delta\theta(r))^4 \rangle$, exhibit inertial-range structure function exponents of 1.36–1.52. However, discrepancies still exist with respect to the various methods used to estimate the scaling exponents, the value of the scalar intermittency exponent, μ_θ, and the effects of large-scale phenomena (namely shear, decay and turbulent production of $\langle \theta^2 \rangle$) on $\langle (\Delta u(r))^2 (\Delta\theta(r))^4 \rangle$. All the measured fine-scale statistics required to be zero in a locally isotropic flow are, or tend towards, zero in the limit of large Reynolds numbers. The probability density functions (PDFs) of $\Delta v(r) \Delta\theta(r)$ exhibit roughly exponential tails for large separations and super-exponential tails for small separations, thus displaying the effects of internal intermittency. As the Reynolds number increases, the PDFs become symmetric at the smallest scales – in accordance with local isotropy. The expectation of the transverse velocity fluctuation conditioned on the scalar fluctuation is linear for all Reynolds numbers, with slope equal to the correlation coefficient between v and θ. The expectation of (a surrogate of) the Laplacian of the scalar reveals a Reynolds number dependence when conditioned on the transverse velocity fluctuation (but displays no such dependence when conditioned on the scalar fluctuation). This former Reynolds number dependence is consistent with Taylor's diffusivity independence hypothesis. Lastly, for the statistics measured, no violations of local isotropy were observed.

1. Introduction

The objective of this work is to examine the variation of mixed (velocity–passive scalar) statistics in grid-generated wind tunnel turbulence with an imposed mean scalar gradient. To this end, probability density functions (PDFs), spectra, structure functions, small-scale statistics and conditional expectations are studied over a wide

range of Reynolds numbers (or Péclet numbers; see below for definitions). Emphasis is placed on the small-scale mixed velocity–passive scalar field and how its behaviour compares with that of the (individual) velocity and passive scalar fields.

To accurately observe any evolution in turbulence statistics with a particular parameter (i.e. the Reynolds number), the parameter should be varied over as large a range as possible. Until recently, the range of obtainable Reynolds numbers in standard laboratory wind tunnels was relatively small – the highest achievable Reynolds numbers were significantly lower than those realized in industrial and geophysical shear flows. However, the development of 'active grids' by Makita (1991) has allowed high-Reynolds-number homogeneous quasi-isotropic decaying turbulence to be achieved in average-size wind tunnels (Makita 1991; Mydlarski & Warhaft 1996, herein referred to as M&W96; Mydlarski & Warhaft 1998*a*, herein referred to as M&W98). In particular, active grids have been used to investigate the effects of variations in Reynolds number on the turbulent velocity field (M&W96) and variations in Péclet number on the turbulent scalar field (M&W98). The velocity field was studied over the range $50 \leqslant R_\lambda \leqslant 473$ in M&W96. (The Taylor-microscale-based Reynolds number, R_λ, is defined by $R_\lambda \equiv u_{rms}\lambda/\nu$, where u is the longitudinal velocity fluctuation, $\lambda \equiv [\langle u^2\rangle/\langle(\partial u/\partial x)^2\rangle]^{1/2}$ and ν is the kinematic viscosity.) The passive scalar field, generated by imposing a linear mean scalar gradient on the same flow as in M&W96, was studied over the range $30 \leqslant R_\lambda \leqslant 731$ ($21 \leqslant Pe_\lambda \leqslant 512$) in M&W98. (The Péclet number is defined as $Pe_\lambda \equiv R_\lambda(\nu/\kappa)$, where κ is the thermal diffusivity.) The present work can be considered as the third element in a study of the effect of the turbulent Reynolds number on velocity and passive scalar statistics.

Before proceeding, it is worthwhile to review briefly the results of M&W96 and M&W98 since they will be compared with the present work. In M&W96, it was shown that the velocity field displayed significant Reynolds number dependence. Namely, at low Reynolds numbers (i.e. $R_\lambda \sim 50$), a weak, poorly defined inertial subrange appeared in the power spectrum of the longitudinal velocity with a slope of about -1.3. By $R_\lambda \sim 200$, a well-defined inertial subrange had developed, with slope of -1.5. At the highest Reynolds numbers achieved, the value of the scaling exponent was approaching, but still significantly below, the $-5/3$ prediction of Kolmogorov (1941*a*, *b*) – also see Monin & Yaglom (1975). The slope of the power spectrum of the transverse velocity evolved even more slowly towards the Kolmogorov prediction. M&W96 also showed that internal intermittency effects were a strong function of Reynolds number. For $R_\lambda < 100$, the effects of internal intermittency were absent from the inertial range. For $R_\lambda > 200$, the magnitude of the effects of internal intermittency increased significantly with Reynolds number. Above, $R_\lambda \sim 200$, Kolmogorov's refined similarity hypothesis (Kolmogorov 1962; Obukhov 1962) was also verified. Lastly, in the limit of large Reynolds numbers, the flow appeared to be locally isotropic. However, no significant large-scale (velocity field) anisotropies were present in this decaying active-grid-generated turbulence to induce small-scale anisotropies of the velocity field.

A significantly different behaviour of the passive scalar field was observed in M&W98. In general, the scalar field showed very little Reynolds/Péclet number dependence. At all Reynolds numbers, the power spectrum of the scalar fluctuations displayed a broad inertial–convective range with scaling exponent close to the Kolmogorov–Obukhov–Corrsin (KOC) prediction of $-5/3$ (Kolmogorov 1941*a*, *b*; Obukhov 1949; Corrsin 1951 – also see Monin & Yaglom 1975). The effects of internal intermittency were observed at all Reynolds numbers and their intensity was not strongly Reynolds number dependent (and roughly equal to that observed in

atmospheric flows). In addition, the passive scalar field exhibited notable Reynolds-number-independent anisotropies – a clear violation of the postulate of local isotropy. Odd-ordered structure functions displayed well-defined scaling regions that scaled in a manner inconsistent with the notion of local isotropy. The scalar derivative skewness (measured in the direction of the mean gradient) was order one and Reynolds-number-independent – notably different from the zero value it must acquire in a locally isotropic flow. The ratio of the temperature derivative standard deviation along the gradient to that normal to the gradient was 1.2 ± 0.1. (In an isotropic flow, it should be 1.)

This anisotropy is probably 'inherited' from the presence of a large-scale anisotropy – the mean temperature gradient. In the velocity field under consideration, no large-scale anisotropy exists to 'contaminate' the small scales. Pumir & Shraiman (1995), Pumir (1996), Garg & Warhaft (1998), Shen & Warhaft (2000), Ferchichi & Tavoularis (2000) and Warhaft & Shen (2001) have studied in detail the postulate of local isotropy in homogeneous shear flow – where a mean velocity gradient is present in one direction. The general consensus is that the velocity field may also exhibit persistent, Reynolds-number-independent anisotropies. However, the velocity field anisotropies are less pronounced since they only occur for higher orders than the anisotropies observed in the scalar field. Shen & Warhaft (2000) find that the velocity field exhibits Reynolds-number-independent anisotropies for odd-orders greater than or equal to 5. The scalar field (e.g. Mestayer *et al.* 1976; Sreenivasan & Antonia 1977; Gibson, Friehe & McConnell 1977; Antonia & Van Atta 1978; Mestayer 1982; Tong & Warhaft 1994; M&W98; Mydlarski & Warhaft 1998*b*) is observed to be anisotropic at the third order – the lowest non-trivial odd order.

The predictions for the behaviour of mixed velocity–passive scalar statistics evolve from the concept of local isotropy and extensions of KOC theory. In particular, the works of Lumley (1964, 1967) predict the following inertial-range scaling of the co-spectrum of velocity (measured in the direction of the mean scalar gradient, v) and temperature (θ) fluctuations:

$$E_{v\theta}(k_1) = C_{v\theta}\beta\langle\epsilon\rangle^{1/3}k_1^{-7/3}, \tag{1.1}$$

where β is the magnitude of the mean scalar gradient, k_1 is the longitudinal wavenumber, $C_{v\theta}$ is a constant and the dissipation of turbulent kinetic energy, $\langle\epsilon\rangle$, is defined as

$$\langle\epsilon\rangle = \frac{\nu}{2}\left\langle\left(\frac{\partial u_i}{\partial x_j} + \frac{\partial u_j}{\partial x_i}\right)\left(\frac{\partial u_i}{\partial x_j} + \frac{\partial u_j}{\partial x_i}\right)\right\rangle; \tag{1.2}$$

ν is the kinematic viscosity of the fluid. Since the present flow is of a low turbulent intensity (i.e. $u_{rms}/\langle U\rangle < 11\%$), Taylor's hypothesis (Taylor 1938) is a reasonable approximation (e.g. Lumley 1965) and is applied through the relationship $k_1 = 2\pi f/\langle U\rangle$, where f is the frequency.

Decaying grid turbulence with an imposed mean temperature gradient has been a turbulent flow of fundamental interest since Corrsin's (1952) prediction that the mean temperature gradient should maintain itself for the length of a wind tunnel (given that the integral length scale of the turbulence is sufficiently smaller than the width of the tunnel). Initially, heated grids were used to generate the mean temperature profile. However, they were shown to result in poor transverse homogeneity of the temperature field (Sirivat & Warhaft 1983). Warhaft & Lumley (1978) and Sirivat & Warhaft (1983) improved upon the homogeneity of the temperature field by introducing two different temperature 'injection' methods: respectively (i) placing an array of fine, heated wires

across the flow downstream of the grid (called a 'mandoline'), and (ii) placing heating elements upstream of the wind tunnel plenum chamber (called a 'toaster'). The second method is used herein to generate the temperature field by imposing a linear mean gradient upon the turbulence. The turbulent velocity field acting against the gradient will create a turbulent temperature field.

The focus of Warhaft & Lumley (1978) was the decay of (isotropic) temperature fluctuations in grid turbulence, with emphasis on the effect of the initial conditions of the injection of the temperature. Sirivat & Warhaft (1983) studied the downstream evolution of the thermal field in decaying grid turbulence with an imposed mean temperature gradient (which therefore adds the effect of turbulent production). The purpose of the present work is to examine the behaviour of mixed velocity–passive scalar statistics, emphasizing their Reynolds number dependence and their small-scale behaviour.

The remainder of the paper is organized as follows. The apparatus is described in § 2. In § 3, we present results for the mixed velocity–passive scalar field over the range $85 \leqslant R_\lambda \leqslant 582$. The results will be compared to the previous results of M&W96 (for the velocity field) and M&W98 (for the passive scalar field). The latter comparison will be of particular interest to determine whether the anisotropies observed in M&W98 are also exhibited in the mixed velocity–passive scalar field. Where appropriate, comparisons will be made with the direct numerical simulations (DNS) of Overholt & Pope (1996, hereinafter referred to as O&P), who examined passive scalar mixing in statistically homogeneous, isotropic, and stationary turbulence with a mean scalar gradient.

2. Apparatus

The mixed velocity–passive scalar statistics presented in this paper are obtained from various experiments performed under the same or similar conditions to those in M&W98. Therefore, the discussion of the apparatus and flow characteristics presented here will only summarize the discussion in M&W98.

The experiments were conducted in two low-speed low-background-turbulence open-circuit wind tunnels in the Sibley School of Mechanical and Aerospace Engineering at Cornell University. One tunnel is horizontal and has dimensions $0.91\,\mathrm{m} \times 0.91\,\mathrm{m} \times 9.1\,\mathrm{m}$; it is described in detail in Yoon & Warhaft (1990). The other tunnel is vertical and has dimensions $0.41\,\mathrm{m} \times 0.41\,\mathrm{m} \times 4.5\,\mathrm{m}$ long. A detailed description is presented in Sirivat & Warhaft (1983).

The standard bi-planar grids used to generate turbulence in wind tunnels were replaced by an active grid, following the design of Makita (1991). Active grids – composed of round grid bars to which are attached triangular agitator wings – enable one to achieve higher turbulent Reynolds numbers in a standard laboratory wind tunnel than by means of 'passive' grids. Stepper motors, located outside the grid, rotate the grid bars. A detailed description of the active grid and its operation is given in M&W96 and M&W98 and is not repeated here.

In both wind tunnels, the mean temperature gradient was produced by means of a *toaster*, first introduced by Sirivat & Warhaft (1983). The toaster, located at the entrance to the wind tunnel plenum chamber, consists of a set of parallel Nichrome ribbons that act as heating elements. The ribbons are equally spaced and span the entire width of the plenum chamber. (Schematics of the two wind tunnels and their respective differential heaters are given in figure 3 of Sirivat & Warhaft (1983) and figure 1 of Yoon & Warhaft (1990).) Air entering the plenum chamber is warmed

as it flows over the (differentially heated) ribbons. Passage of the air though the honeycombs, screens, etc. (located in the plenum) smoothes out the (momentum and thermal) wakes of the heater ribbons. The air then passes through the contraction and over the grid (located at the entrance to the test section of the wind tunnel). The resulting turbulent flow downstream of the grid has an imposed temperature gradient. Its linearity is ensured by iteratively adjusting the electric current passing through each element of the toaster. The mean flow is in the x_1- (longitudinal) direction and the mean temperature gradient is in the x_2- (transverse) direction. The resulting temperature fluctuations can be considered passive since the buoyant production of velocity fluctuations is negligible (see M&W98).

Velocity fluctuations were measured by means of Dantec 55M01 constant-temperature hot-wire anemometers (operated at an overheat ratio of 1.8) using TSI 1241 X-wire probes. The hot wires were made from 3.05 μm diameter tungsten with a length to diameter ratio of approximately 200. The X-wires were calibrated following the effective angle method of Browne, Antonia & Chua (1989). Compensation of the velocity measurements for temperature fluctuations was effected by means of a modified King's Law with temperature-dependent coefficients (Lienhard 1988). The two wires comprising the X-wire were separated by 0.5 mm.

The temperature fluctuations were measured by a cold wire placed 0.5 mm away from the X-wire. The cold wires were made from Wollaston wire, with a 0.63 μm diameter platinum core, soldered to a TSI 1210 single-wire probe. The ratio of the etched length of the wire to its diameter varied from 500 to 650 and the spacing between the prongs was at least three times the etched length. Fast-response DC temperature bridges (based on the design of Haughdal & Lienhard 1988) were used to measure the temperature fluctuations. The probe current through the cold-wire thermometer sensors was approximately 250 μA.

The frequency response of the probes and the cold-wire thermometers is addressed in M&W98. They also discuss the optimal choice of cold-wire length given the competing effects of spatial resolution and conduction between the cold wire and its prongs. The discussion (not repeated here) shows that there are no serious temporal resolution effects and that the chosen cold-wire length is optimal since we are interested in both the small- and large-scale statistics of the temperature field.

The output from the hot-wire anemometers and cold-wire thermometers was both high- and low-pass filtered. The signals were digitized using a 12-bit A/D converter. Each record consisted of 4 or 8×10^5 data points. For time-series measurements (used in the calculations of longitudinal derivatives, spectra, etc.) the data were sampled at twice the low-pass filter frequency (which was set to a value slightly higher than the Kolmogorov frequency). Time derivatives were numerically calculated using an $O(h^4)$ centred finite difference formula. The derivative statistics presented in § 3.3 exhibited no significant variation when the sampling rate was, as a test, halved. Taylor's hypothesis (Taylor 1938) is used to convert temporal increments and derivatives into spatial ones. For PDF measurements, the data were sampled at intervals on the order of an integral time period.

Table 1 lists the flow parameters. The turbulent quantities presented in this table have had the effects of the low-wavenumber spikes present in the spectra (an artifact of the active grid) subtracted (on a mean-square basis). This results in a more realistic description of the turbulence and the procedure is described in detail in M&W96, p. 338. These spikes occur at scales much larger than the integral scale (i.e. they occur at frequencies much smaller than those corresponding to the integral scale) and do not affect the turbulence (M&W96; M&W98). We emphasize the non-

Mean speed [$\mathrm{m\,s^{-1}}$]	3.3	3.3	12.2	3.3	11.4	7.0
x/M	68	62	68	62	68	62
Tunnel	V	H	V	H	V	H
β $(=\partial\langle T\rangle/\partial y)$ [$^\circ\mathrm{C\,m^{-1}}$]	4.8	2.5	5.2	2.7	3.6	3.6
ν [$\mathrm{m^2\,s^{-1}}$]	16×10^{-6}	15.5×10^{-6}	16×10^{-6}	16×10^{-6}	16×10^{-6}	16×10^{-6}
$\langle u^2\rangle$ [$(\mathrm{m\,s^{-1}})^2$]	0.0156	0.0290	0.311	0.0911	1.04	0.583
$\langle v^2\rangle$ [$(\mathrm{m\,s^{-1}})^2$]	0.0133	0.0209	0.267	0.0594	0.828	0.424
$\langle\epsilon\rangle$ $(=15\nu\int_0^\infty k_1^2E_u(k_1)\,\mathrm{d}k_1)$ [$\mathrm{m^2\,s^{-3}}$]	0.0314	0.0418	2.33	0.0833	6.13	0.940
ℓ $(=0.9\langle u^2\rangle^{3/2}/\epsilon)$ [m]	0.056	0.11	0.067	0.30	0.16	0.43
W/ℓ	7.3	8.3	6.1	3.0	2.6	2.1
R_λ $(=\langle u^2\rangle(15/(\nu\epsilon))^{1/2})$	85	140	197	306	407	582
R_ℓ $(=u_{rms}\ell/\nu)$	440	1200	2300	5600	9900	20 300
η $(=(\nu^3/\epsilon)^{1/4})$ [mm]	0.60	0.55	0.21	0.47	0.16	0.26
$\langle\theta^2\rangle$ [$(^\circ\mathrm{C})^2$]	0.062	0.176	0.055	0.800	0.080	1.07
$\langle\epsilon_\theta\rangle$ $(=3.4\kappa\langle(\partial\theta/\partial x)^2\rangle)$ [$^\circ\mathrm{C^2\,s^{-1}}$]	0.062	0.138	0.200	0.399	0.233	0.870
ℓ_θ $(=\theta_{rms}/\beta)$ [m]	0.052	0.17	0.045	0.33	0.079	0.29
R $(=((\langle u^2\rangle+2\langle v^2\rangle)/\langle\epsilon\rangle)/(\langle\theta^2\rangle/\langle\epsilon_\theta\rangle))$	1.34	1.33	1.32	1.26	1.28	1.24
$\langle v\theta\rangle$ [$^\circ\mathrm{C\,m\,s^{-1}}$]	−0.0216	−0.0213	−0.0576	−0.0407	−0.100	−0.137
$\rho_{v\theta}$	−0.75	−0.35	−0.48	−0.19	−0.39	−0.20

TABLE 1. Flow parameters for some representative cases. M represents the mesh length of the active grid, 0.114 m (= 4.5 in.) for the horizontal (H) tunnel and 0.0508 m (= 2 in.) for the vertical (V) one. W is the tunnel width – given in § 2. Turbulent quantities in this table were determined by subtracting, on a mean-square basis, the effect of the low-wavenumber spikes present in the spectra (an artifact of the active grid – see text). The factor of 3.4 in the definition of $\langle\epsilon_\theta\rangle$ is due to the anisotropic nature of the scalar derivative in flows with mean scalar gradients. The thermal diffusivity, κ, was $22.5\times10^{-6}\,\mathrm{m^2\,s^{-1}}$.

standard definition of $\langle\epsilon_\theta\rangle$ (given in table 1) that accounts for the anisotropy of a passive scalar in a turbulent flow with a mean temperature gradient. This anisotropy, $(\langle(\partial\theta/\partial y)^2\rangle/\langle(\partial\theta/\partial x)^2\rangle\simeq1.4)$, is explored in detail in Tong & Warhaft (1994) and M&W98.

3. Results

Similar to the velocity field in M&W96 and to the passive scalar field in M&W98, the objective of this work is to study the evolution of mixed (velocity–passive scalar) statistics in grid-generated turbulence over a wide range of Reynolds numbers ($85\leqslant R_\lambda\leqslant582$). To this end, some large-scale statistics are presented in § 3.1. The remaining sections of the paper treat inertial- and dissipative-range statistics, reported in terms of spectra and structure functions (§ 3.2), the small-scale structure (§ 3.3) and conditional statistics (§ 3.4). Appendix A contains a comparison of the scaling exponents of $\langle(\Delta u)^2(\Delta\theta)^4\rangle$ with two models. Some (solely) scalar conditional expectations are discussed in Appendix B.

3.1. *Large-scale mixed velocity–passive scalar statistics*

The details of the flow characteristics are given (for the velocity field) in M&W96 and (for the scalar field) in M&W98. The present velocity field is close to Gaussian (M&W96 – figure 5) while the temperature field is slightly sub-Gaussian with a kurtosis

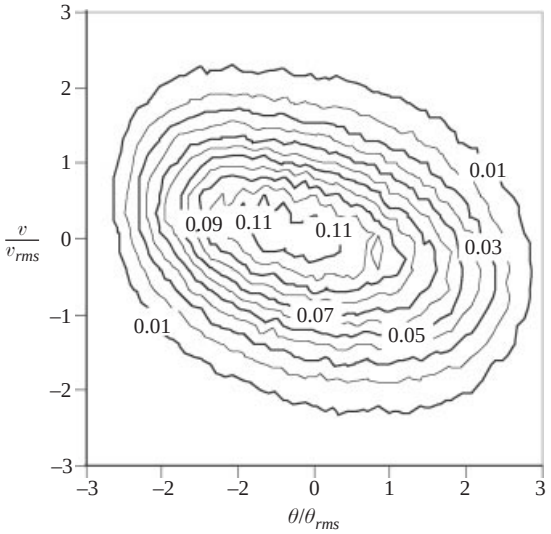

FIGURE 1. A typical joint probability density function of the turbulent transverse velocity fluctuation, v, and the turbulent temperature fluctuation, θ. $R_\lambda = 582$.

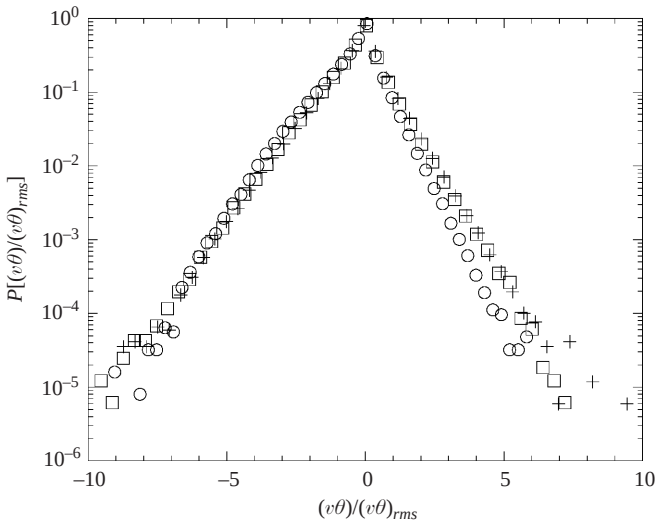

FIGURE 2. Probability density functions of the turbulent heat flux, $v\theta$: ○, $R_\lambda = 140$; +, $R_\lambda = 306$; □, $R_\lambda = 582$.

of approximately 2.3 (M&W98 – figure 2). Here, we present the (normalized) joint PDF of v and θ in figure 1. (In the flow under consideration, u and v, as well as u and θ, are uncorrelated. It is therefore unnecessary to show their respective joint PDFs.) Given the sub-Gaussian nature of the scalar field, the joint PDFs exhibit slight deviations from a joint-Gaussian distribution (e.g. the major axes of the ellipses formed by contour lines are not parallel to the $y = -x$ line, etc.). Such a result was typical for all Reynolds numbers. The only variation was in the 'width' of the ellipses formed by contour lines of the joint PDFs. This results from differences in the correlation coefficient $\rho_{v\theta} \equiv \langle v\theta \rangle / (v_{rms}\theta_{rms})$ (discussed below).

As was shown by Thoroddsen & Van Atta (1992), exponential tails for the PDF of $v\theta$ can be predicted given a joint-Gaussian behaviour of v and θ. Figure 2 shows

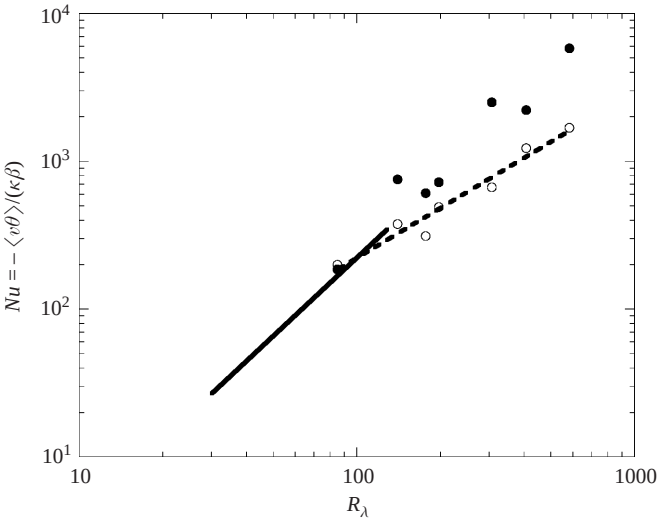

FIGURE 3. The turbulent Nusselt number as a function of Reynolds number for decaying grid turbulence with an imposed mean (passive) temperature gradient. Solid line: the best-fit power law to the data of Jayesh & Warhaft (1992); ○, present work; ●, present work assuming $\rho_{v\theta} = -0.7$; dashed line; the best-fit ($R_\lambda^{1.1}$) power law to the present data.

the (normalized) PDFs of the turbulent heat flux, $v\theta$, for three Reynolds numbers ($R_\lambda = 140, 306$ and 582). These PDFs collapse relatively well, though the positive tail for the lowest Reynolds number falls off at a slightly higher rate than for the other two Reynolds numbers. The tails of the PDF are approximately exponential (with the negative one less steeply sloped than the positive one because of the nature of the flow – $v\theta$ is more likely to be negative than positive). Such a result is expected, given the quasi-joint-Gaussian nature of the flow.

We plot in figure 3 the turbulent Nusselt number ($Nu \equiv -\langle v\theta\rangle/(\kappa\beta)$) as a function of R_λ. On the same figure is plotted the best fit line to the results of Jayesh & Warhaft (1992). Before proceeding, we make two comments. First, the data of Jayesh & Warhaft (1992) has been transformed from R_ℓ to R_λ by the relation $R_\ell = \frac{0.9}{15}R_\lambda^2$ (Tennekes & Lumley 1972; M&W96). Secondly, Jayesh & Warhaft (1992) determined $\langle v\theta\rangle$ by assuming that $u_{rms} \sim v_{rms}$ and that $\rho_{v\theta} = -0.7$. We observe that the lowest Reynolds number data of the present work are in agreement with the data of Jayesh & Warhaft (1992). However, the present data exhibit an $R_\lambda^{1.1}$ power law behaviour while the data of Jayesh & Warhaft (1992) display an $R_\lambda^{1.76}$ dependence. It is unlikely that a transition is occurring at $R_\lambda \sim 100$. The more likely explanation is that the lower slope arises from a dependence of $\rho_{v\theta}$ on the Reynolds number and/or the ratio of the tunnel width (W) to the integral length scale (ℓ) of the flow (see table 1).

Also shown in figure 3 is the Nusselt number calculated from $Nu = -\rho_{v\theta}v_{rms}\theta_{rms}/(\kappa\beta)$ assuming $\rho_{v\theta} = -0.7$. This exhibits an $R_\lambda^{1.7}$ power law dependence and follows the trend of the data of Jayesh & Warhaft (1992). The difference between the two Nu curves lies in the changes in $\rho_{v\theta}$. It is still unclear whether this is an artifact of the lower W/ℓ ratios in this flow or whether this is related to the increasing Reynolds number (or both). High-Reynolds-number experiments with large W/ℓ would serve to clarify this relationship. Such experiments are, unfortunately, not practical since $R_\ell \propto \ell$. We also point out that O&P observe a decay in $\rho_{v\theta}$ from -0.603 at $R_\lambda = 28$ to -0.464 at $R_\lambda = 185$. However, their numerical simulations also suffer from a low ratio of the computational domain width to the integral length scale.

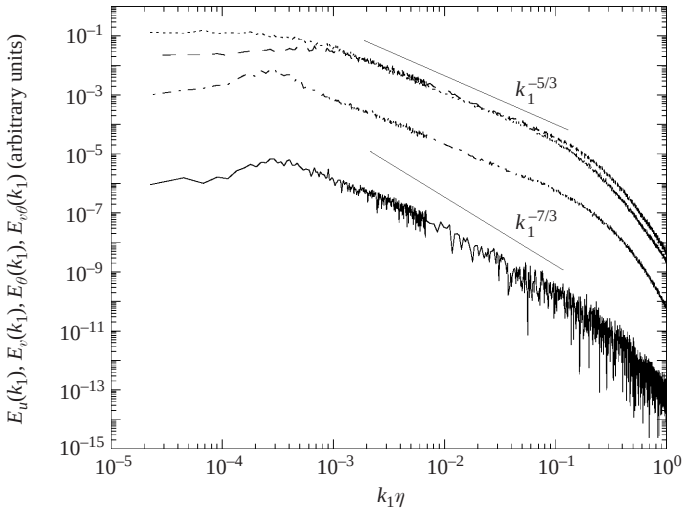

FIGURE 4. Spectra at $R_\lambda = 582$. The power spectrum of longitudinal velocity fluctuations, $E_u(k_1)$ (short-dashed line), the power spectrum of transverse velocity fluctuations, $E_v(k_1)$ (long-dashed line), the power spectrum of temperature fluctuations, $E_\theta(k_1)$ (dot-dashed line) and the co-spectrum of the transverse velocity and temperature fluctuations, $E_{v\theta}(k_1)$ (solid line).

Next, we consider the ratio of the mechanical to thermal time scale,

$$R \equiv (\langle u_i u_i \rangle / \langle \epsilon \rangle)/(\langle \theta^2 \rangle / \langle \epsilon_\theta \rangle) = ((\langle u^2 \rangle + 2\langle v^2 \rangle)/\langle \epsilon \rangle)/(\langle \theta^2 \rangle / \langle \epsilon_\theta \rangle),$$

where the last equation assumes an axisymmetric flow. The time scale ratio is found to be 1.28 ± 0.07 and roughly independent of R_λ. This value compares well with the equilibrium value of 1.4–1.6 (for temperature fluctuations generated by means of a mandoline or a toaster) obtained in Sirivat & Warhaft (1983) for grid-generated turbulence with a mean scalar gradient. The Reynolds number independence of R (for R_λ greater than approximately 10^2) is consistent with the results of Pullin (2000) and Xu, Antonia & Rajagopalan (2000*b*). Using large-eddy simulation with stretched-vortex subgrid stress models, Pullin (2000) obtains a mechanical to thermal time-scale ratio that asymptotes to $R \approx 2.8$ for $R_\lambda > 180$. (The asymptotic value of R is flow dependent. It is the Reynolds number dependence of R with which we are concerned here.) Xu *et al.* (2000*b*) develop an expression for R (based on structure function parameterization) and, comparing their results with various sets of data, come to the conclusion that R should tend to a constant value in the limit of large Reynolds numbers. From their work, $R_\lambda \sim 100$ appears to be large enough for R to tend to a constant value. We remark that the time scale ratio used in Xu *et al.* (2000*b*) is defined slightly differently.

Lastly, we mention that there exists a relationship between R and the rates of change of turbulent kinetic energy ($\langle u_i u_i \rangle$) and scalar variance ($\langle \theta^2 \rangle$) in the downstream direction. For grid turbulence with imposed isotropic temperature fluctuations, the relationship has been presented in Zhou *et al.* (2000). In such a flow, the kinetic energy decays. However, when a mean scalar gradient is present, the scalar variance can increase with x_1/M, unlike in Warhaft & Lumley (1978) or Zhou *et al.* (2000). The downstream evolutions of $\langle u_i u_i \rangle$ and $\langle \theta^2 \rangle$ for experiments similar to the present ones are discussed in M&W96, M&W98 and in section II of Danaila & Mydlarski (2001). They are not the focus of the present work and, as such, their relationship to R is not determined herein.

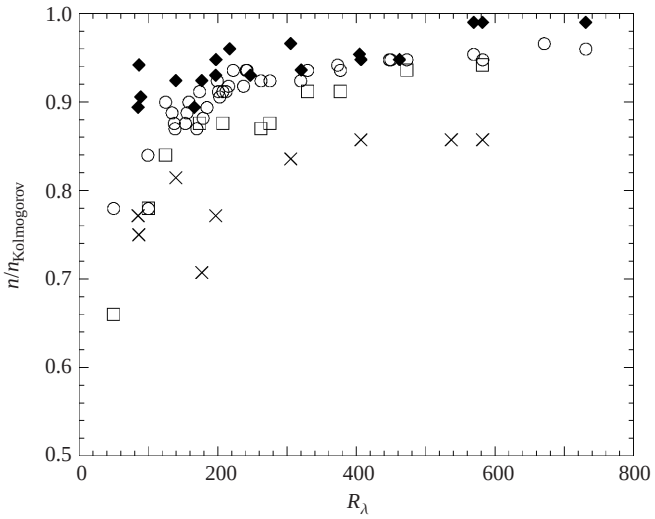

FIGURE 5. Non-dimensionalized spectral slopes as a function of R_λ: ○, the longitudinal velocity spectrum slope (n_u); □, the transverse velocity spectrum slope (n_v); ◆, the temperature spectrum slope (n_θ); ×, the slope of the co-spectrum of transverse velocity and temperature ($n_{v\theta}$).

3.2. *The spectra and structure functions*

Figure 4 shows four (one-dimensional) spectra at $R_\lambda = 582$: the power spectrum of longitudinal velocity fluctuations, $E_u(k_1)$; the power spectrum of transverse velocity fluctuations, $E_v(k_1)$; the power spectrum of temperature fluctuations, $E_\theta(k_1)$; and the co-spectrum of the transverse velocity and temperature fluctuations, $E_{v\theta}(k_1)$. For the range of scales $1 \times 10^{-4} < \kappa_1\eta < 6 \times 10^{-4}$, a slight bump is present in the power spectrum of temperature and the co-spectrum of transverse velocity and temperature. These are an artifact of the active grid and do not significantly affect the flow since they occur at scales larger than the integral scale (as discussed in § 3 of M&W98). The co-spectrum is noisier than the three power spectra since it has no mathematical limitation preventing it from taking on negative values. To plot the co-spectrum in log-log coordinates, the occasional negative excursion has been removed.

At this relatively large Reynolds number, all four spectra show broad scaling ranges in the inertial subrange. Kolmogorov (1941*a*, *b*) predicted that, in the limit of infinite Reynolds number, the slope of $E_u(k_1)$ and $E_v(k_1)$ should be equal to $-5/3$ in the inertial range. Following the notions of Kolmogorov, Obukhov (1949) and Corrsin (1951) came to the same conclusion for the temperature spectrum. Lumley (1964, 1967) postulated that the co-spectrum of velocity and temperature should have a slope equal to $-7/3$ in the inertial subrange. Figure 5 shows the Reynolds number dependence of the inertial-range slopes for the power spectra of longitudinal velocity (n_u), transverse velocity (n_v), temperature (n_θ) and for the co-spectra of transverse velocity and temperature ($n_{v\theta}$), as measured in M&W96 and M&W98. The slopes are non-dimensionalized by their high-Reynolds-number prediction (i.e. $-5/3$ for n_u, n_v and n_θ; $-7/3$ for $n_{v\theta}$). In figure 5, one observes the already-mentioned different scaling-exponent evolution of n_u and n_v compared to that of n_θ, (i.e. n_v tends to a value of $-5/3$ more slowly than that n_u, which does so more slowly than n_θ). The scaling-range exponent of the co-spectra ($n_{v\theta}$) more closely resembles that of the velocity field than the scalar field, given its slow evolution and that, even at the highest Reynolds numbers, it is significantly different from Lumley's (1964, 1967)

$-7/3$ prediction. The retarded evolution of $n_{v\theta}$ seems to indicate that the co-spectrum is dominated by its contribution from the velocity field.

We also point out that even though the evolution of $n_{v\theta}$ is slow, the (dimensional) value of $n_{v\theta}$ is nevertheless greater than both n_v and n_θ for all Reynolds, indicating a tendency towards local isotropy (at least with respect to second-order quantities like the spectra).

Tavoularis & Corrsin (1981) measured the co-spectrum of the transverse velocity and temperature fluctuations in homogeneous shear flow with an imposed mean temperature gradient (in the same direction as the shear). At $R_\lambda = 266$, they observed a scaling range with a slope approximately equal to -1.5 (i.e. $n_{v\theta}/(-7/3) \approx 0.64$). This is slightly lower than observed herein. However, given that the spectrum of the scalar evolves very differently in shear flows†, such a result could be expected presuming a correlation between the evolution of the individual velocity and scalar fields and that of the combined fields. Co-spectra of transverse velocity and temperature were also presented in Yoon & Warhaft (1990) and Lienhard & Van Atta (1990). The Reynolds number of these flows was, however, too low for the co-spectrum to exhibit a scaling range with a distinct slope.

P. A. O'Gorman and D. I. Pullin (private communication), using the stretched-spiral vortex model, have calculated the velocity–scalar co-spectrum for homogeneous isotropic turbulence in the presence of a mean scalar gradient. They obtained an asymptotic expression for the co-spectrum of the scalar and axial velocity component (of the stretched-spiral vortex) with a leading-order term proportional to $k^{-5/3}$. The next-order term exhibited a $k^{-7/3}$ dependence. These results are not inconsistent with the scaling-range slope of -2.0 (i.e. $n_{v\theta}/(-7/3) \approx 0.86$) observed in the present work at high Reynolds number.

The imaginary component of the cross-spectral density function, the quadrature spectrum ($Q_{v\theta}(k_1)$), is also calculated and found to be effectively zero (until noise effects become significant at small scales, i.e. $k_1\eta \gtrsim 0.1$). Consequently, the resulting phase angle between v and θ, $Ph_{v\theta}(k_1) \equiv \tan^{-1}(Q_{v\theta}(k_1)/E_{v\theta}(k_1))$, is roughly 180° over all wavenumbers until the signal-to-noise ratio falls and noise begins to dominate.

Figure 6 shows $\langle \Delta v(r)\Delta\theta(r)\rangle$ (where $\Delta v \equiv v(x+r) - v(x)$ and $\Delta\theta \equiv \theta(x+r) - \theta(x)$) plotted as a function of separation for various Reynolds numbers. Figure 6(a) plots the non-dimensional structure functions in an uncompensated form while figure 6(b) presents them in compensated form. We choose to call measurements of $\langle \Delta v(r)\Delta\theta(r)\rangle$ 'heat flux structure functions' since they are related to the turbulent transport of temperature by eddies of size r. In the limit of large separations (i.e. as $r \to \infty$), they are equal to twice the turbulent heat flux, $2\langle v\theta\rangle = 2\langle u_2\theta\rangle$. In the limit of small separations (i.e. as $r \to 0$), they display an r^2 behaviour, as expected.

The heat flux structure function is the real-space analogue of the (one-dimensional) co-spectrum of velocity and temperature, $E_{v\theta}(k_1)$. Lumley's (1964, 1967) $-7/3$ prediction translates to a $4/3$ ($= -1 \times (-7/3 + 1)$) inertial-range slope of $\langle \Delta v(r)\Delta\theta(r)\rangle$. The observed heat flux structure function scaling exponents (determined by compensation of the structure functions) are 0.75 at $R_\lambda = 85$, 0.80 at $R_\lambda = 197$ and 1.02 at $R_\lambda = 407$. These values are in reasonable agreement with the values of $n_{v\theta}$ from figure 5 and may be slowly approaching their theoretical prediction of $4/3$ as the Reynolds number

† It has been observed (e.g. Sreenivasan 1991) that in shear flows, the scaling exponent of the power law region of the scalar power spectrum evolves slowly with Reynolds number and only approaches the Kolmorogov prediction of $-5/3$ at very high Reynolds numbers (i.e. $R_\lambda > 10^3$). This is in sharp contrast to the power spectrum of the scalar in isotropic flows which exhibits a $-5/3$ scaling region at low Reynolds numbers (i.e. $R_\lambda < 50$ (Jayesh, Tong & Warhaft 1994)).

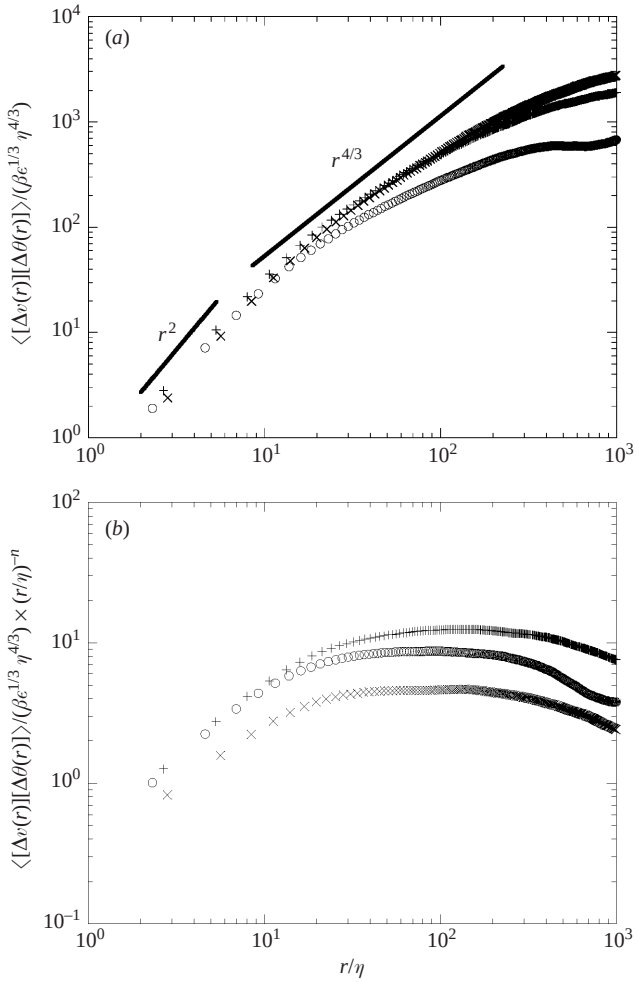

FIGURE 6. The 'heat flux structure functions', $\langle\Delta v(r)\Delta\theta(r)\rangle$ in (a) uncompensated and (b) compensated form. ○, $R_\lambda = 85$, $n = 0.75$; +, $R_\lambda = 197$, $n = 0.80$; ×, $R_\lambda = 407$, $n = 1.02$.

is increased. We remark that the non-dimensionalization employed in figure 6(a) – a non-dimensionalization that, other than the linear dependence on β, is in terms of small-scale variables – collapses the data only up to separations of $r/\eta \sim 15$. No collapse of the data in the inertial-range occurs, because the inertial-range scaling exponent has yet to asymptote to a constant value.

Two additional comments should be made. First, we only present results for the heat flux structure functions in the y-direction since this is the only direction in which a mean scalar gradient is present. Secondly, we have measured the *longitudinal* structure function of the *transverse* turbulent heat flux, $\langle\Delta v(x)\Delta\theta(x)\rangle$. The transverse structure functions of the transverse turbulent heat flux ($\langle\Delta v(y)\Delta\theta(y)\rangle$) are slightly different, as can be seen in figure 1 of Danaila & Mydlarski (2001), who present DNS results provided by A. Pumir. We are unable to measure $\langle\Delta v(y)\Delta\theta(y)\rangle$ with the present apparatus.

At the next order, we discuss the third-order longitudinal mixed structure function, $\langle\Delta u(r)(\Delta\theta(r))^2\rangle$, where $\Delta u \equiv u(x+r) - u(x)$ and $\Delta\theta \equiv \theta(x+r) - \theta(x)$. For homo-

geneous isotropic quasi-stationary turbulence in the limit of infinite Reynolds number, Yaglom (1949) derived (from the advection–diffusion equation for a passive scalar) an expression for $\langle \Delta u(\Delta\theta)^2 \rangle$:

$$\langle \Delta u(r)(\Delta\theta(r))^2 \rangle = 2\kappa \frac{\mathrm{d}}{\mathrm{d}r} \langle (\Delta\theta(r))^2 \rangle - \tfrac{4}{3} \langle \epsilon_\theta \rangle r. \tag{3.1}$$

For inertial-range separations, this expression reduces to what is now known as 'Yaglom's four-thirds law':

$$\langle \Delta u(r)(\Delta\theta(r))^2 \rangle = -\tfrac{4}{3} \langle \epsilon_\theta \rangle r. \tag{3.2}$$

M&W98 plotted (non-dimensionalized) $\langle \Delta u(\Delta\theta)^2 \rangle$ as a function of separation for various Reynolds numbers. (A similar plot is not reproduced here.) They observed that $\langle \Delta u(\Delta\theta)^2 \rangle$ only tends to the prediction of Yaglom (i.e. $-4/3$) for large Reynolds numbers. It has recently been shown by Danaila *et al.* (1999) (for an isotropic flow with isotropic temperature fluctuations) that the non-stationarity of a flow (such as the decay of grid turbulence) causes a deviation of $\langle \Delta u(\Delta\theta)^2 \rangle$ from $-\frac{4}{3}\langle \epsilon_\theta \rangle r$ in the inertial range at low Reynolds numbers. This effect was accounted for by deriving a generalized form of Yaglom's equation in which the non-stationary term was retained. In a similar manner, the (additional) effect of production of scalar fluctuations by a mean gradient (as is the case here) was also shown to affect the value of $\langle \Delta u(\Delta\theta)^2 \rangle$ in the inertial-range at low Reynolds numbers (see Danaila & Mydlarski 2001). These effects occur at the largest scales for any Reynolds number. At low Reynolds numbers (i.e. when the separation of scales is small), the non-stationarity and production therefore also 'contaminate' the smaller (i.e. inertial and dissipative) scales. It is these phenomena which cause the deviations from 4/3 in figure 19 of M&W98.

Finally in this section, in figure 7(*a*), we plot the sixth-order longitudinal mixed structure function, $\langle (\Delta u(r))^2 (\Delta\theta(r))^4 \rangle$, for various Reynolds numbers. It is of particular physical interest since $((\Delta u)^2(\Delta\theta)^4)$ can be viewed as the square of the transport of scalar variance by an eddy of size r. The deviation of its scaling exponent from the KOC prediction of 2 can be used to estimated the scalar intermittency exponent, μ_θ, which is determined from the autocorrelation of the scalar dissipation:

$$\rho_{\epsilon_\theta \epsilon_\theta}(r) = \frac{\langle \epsilon_\theta(x) \epsilon_\theta(x+r) \rangle}{\langle \epsilon_\theta^2 \rangle} \propto r^{-\mu_\theta}, \tag{3.3}$$

where r is an inertial–convective subrange distance. (This is described, for example, in Antonia *et al.* 1984.) In figure 7(*b*), the higher Reynolds number structure functions are plotted in compensated form.

There appear to be only five sets of measurements of $\langle (\Delta u)^2 (\Delta\theta)^4 \rangle$ by three different research groups (namely Chambers & Antonia 1984; Zhu, Antonia & Hosokawa 1995; Schmitt *et al.* 1996; Lévêque *et al.* 1999; Xu, Antonia & Rajagopalan 2000). The data of Xu *et al.* (2000) are included in figure 7. All five sets of measurements are made in flows with mean temperature gradients. The sixth-order mixed structure function was also estimated in the DNS of Boratav & Pelz (1998), where no large-scale anisotropy was present.

As with the measurements of $\langle \Delta u(\Delta\theta)^2 \rangle$ in M&W98, there is a noticeable variation in the inertial-range behaviour of $\langle (\Delta u)^2 (\Delta\theta)^4 \rangle$ with Reynolds number. The inertial-range exponents (estimated by direct compensation of the structure functions) were 1.46 at $R_\lambda = 306$, 1.36 at $R_\lambda = 407$ and 1.52 at $R_\lambda = 582$. No significant scaling range in $\langle (\Delta u)^2 (\Delta\theta)^4 \rangle$ was present at the lower Reynolds numbers and therefore no scaling exponent could be estimated. (At the sixth order, the scaling-range exponents can only

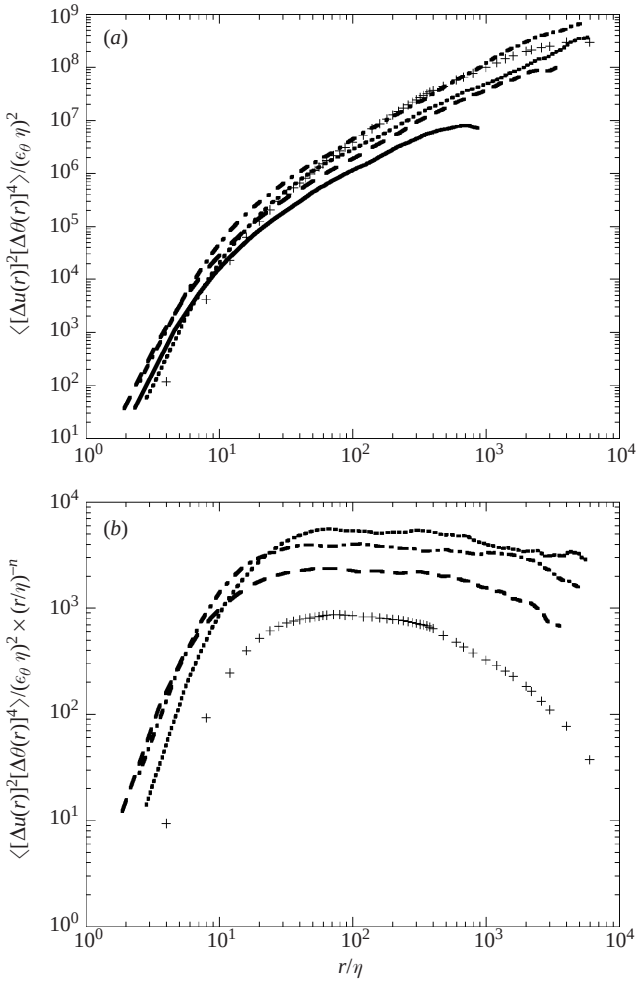

FIGURE 7. The non-dimensionalized sixth-order mixed velocity–temperature structure function, $\langle(\Delta u(r))^2(\Delta\theta(r))^4\rangle$ in (*a*) uncompensated and (*b*) compensated form. Solid line: $R_\lambda = 85$; long-dashed line: $R_\lambda = 306$, $n = 1.46$; short-dashed line: $R_\lambda = 407$, $n = 1.36$; dot-dashed line: $R_\lambda = 582$, $n = 1.52$. +, The turbulent round jet data ($R_\lambda = 550$, $n = 1.83$) of Xu *et al.* (2000*a*).

be estimated with an accuracy of ± 0.05.) The inertial-range scaling exponents, estimated by extended self-similarity (ESS – Benzi *et al.* 1993) conditioned on $\langle|\Delta u(\Delta\theta)^2|\rangle$, were 1.55 at $R_\lambda = 85$, 1.55 at $R_\lambda = 306$, 1.67 at $R_\lambda = 407$ and 1.58 at $R_\lambda = 582$. The values determined by ESS are higher than those determined directly since $\langle|\Delta u(\Delta\theta)^2|\rangle$ does not scale as $r^{1.0}$ in the inertial range (not shown). Rather $\langle|\Delta u(\Delta\theta)^2|\rangle$ scales as 0.90 ± 0.05 in the inertial range for the Reynolds numbers under consideration.

Chambers & Antonia (1984) (along with Zhu *et al.* (1995), who use data from the same set of experiments) obtain a scaling exponent of 1.75 ± 0.05 for $\langle(\Delta u)^2(\Delta\theta)^4\rangle$ (estimated by structure function compensation) in atmospheric surface layer measurements at $R_\lambda = 4298$–7830. Schmitt *et al.* (1996) obtain a scaling exponent of 1.65 ± 0.05 (by least-squares regression in the inertial range) in atmospheric surface layer measurements at an unspecified, but presumably high, R_λ – the dissipative scales were not resolved by the sonic anemometer. Lévêque *et al.* (1999) obtain a scaling exponent of 1.608 ± 0.028 (estimated by ESS conditioned on $\langle|\Delta u(\Delta\theta)^2|\rangle$) in the heated wake of

a cylinder at $R_\lambda \approx 300$. Xu *et al.* (2000*a*) obtain a scaling exponent of 1.83 (estimated by least-squares regression) in a turbulent round jet at $R_\lambda = 550$. In their (isotropic) simulations at $R_\lambda = 99$ and 141, Boratav & Pelz (1998) estimate the inertial-range scaling exponent of $\langle(\Delta u)^2(\Delta\theta)^4\rangle$, by means of ESS conditioned on $\langle|\Delta u(\Delta\theta)^2|\rangle$, to be 1.61 ± 0.04.

The scaling exponents in the present work (particularly when determined by ESS) are in better agreement with the experiments of Lévêque *et al.* (1999) and Schmitt *et al.* (1996) than with Chambers & Antonia (1984), Zhu *et al.* (1995) and Xu *et al.* (2000*a*). It is unclear to what the difference can be attributed. Some of the disparity may arise from the use of different methods to determine the scaling exponents. Direct measurement of the scaling exponents is preferable. However, such a method is limited to high Reynolds numbers, where a large enough scaling range must be present to make a reasonable estimate of its power-law slope. On the other hand, ESS cannot be used without caution at low Reynolds numbers because the third-order structure function only scales as $r^{1.0}$ for large Reynolds numbers (M&W96; M&W98). Additionally, all the previous measurements of $\langle(\Delta u)^2(\Delta\theta)^4\rangle$ were made in shear flows. Like the scalar power spectrum, there may be a significant difference in the behaviour of $\langle(\Delta u)^2(\Delta\theta)^4\rangle$ in shear and shear-free flows. The present experiments appear to produce scaling exponents that are lower than those observed in shear flows.

The scaling exponents measured herein are compared with the log-normal model (Xu *et al.* 2000*a*) and the hierarchical structure model of Lévêque *et al.* (1999) in Appendix A.

3.3. *The fine-scale structure*

We now proceed to study the Reynolds number dependence of the small-scale structure of the flow. Another aim of this subsection, though not unrelated, is to determine whether the mixed velocity–temperature field displays any small-scale anisotropies. In this flow, the scalar field is anisotropic and the velocity field is isotropic. It will be therefore of interest to compare, from an isotropy point of view, the mixed velocity–passive scalar field with the (individual) velocity and passive scalar fields.

We begin by plotting the correlation coefficient between longitudinal derivatives of transverse velocity and temperature:

$$\rho_{\partial v/\partial x,\partial\theta/\partial x} \equiv \frac{\langle(\partial v/\partial x - \langle\partial v/\partial x\rangle)(\partial\theta/\partial x - \langle\partial\theta/\partial x\rangle)\rangle}{(\partial v/\partial x)_{rms}(\partial\theta/\partial x)_{rms}}, \tag{3.4}$$

as a function of Reynolds number, R_λ, in figure 8. As for the heat flux structure functions, we only plot the correlation with the velocity component in the direction of the mean gradient. (In fact, the above correlation coefficient is equal to the non-dimensional heat flux structure function in the limit of small separations.) In a locally isotropic flow, equation (3.4) must tend to zero in the limit of infinite Reynolds number. This appears to be the case, as can be seen in figure 8. Included in this figure are results from the DNS of O&P. Their data span the range $28 \leqslant R_\lambda \leqslant 185$. The present results extend from $R_\lambda = 85$ to $R_\lambda = 582$. For the range of Reynolds numbers where both sets of results overlap, the agreement is reasonable. Overall, the correlation coefficient appears to decrease with R_λ following a power law of slope approximately equal to -0.7 to -0.9, depending on whether the two outlying data points are included in the least-squares fit.

It would be of interest to determine the correlation coefficients of mixed derivative statistics containing transverse derivatives of temperature (e.g. $\rho_{\partial v/\partial x,\partial\theta/\partial y}$, $\rho_{\partial v/\partial y,\partial\theta/\partial y}$, etc.). Statistics of this nature are more likely to detect the anisotropy of the scalar field,

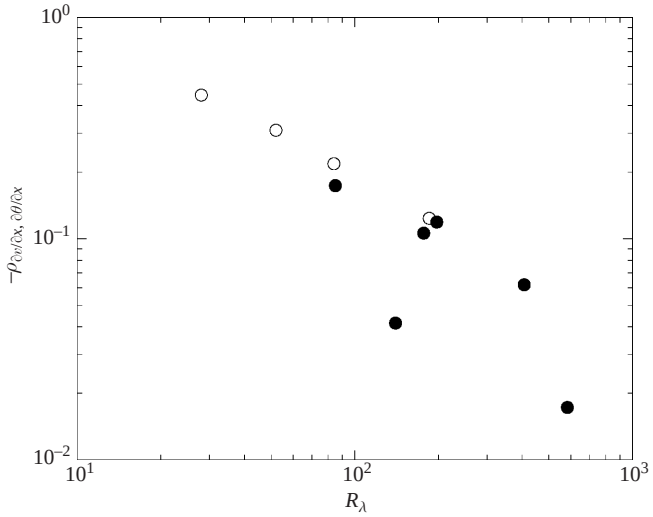

FIGURE 8. The negative of the correlation coefficient between $\partial v/\partial x$ and $\partial\theta/\partial x$ as a function of Reynolds number; ●, present work; ○, DNS of O&P.

given that the mean scalar gradient is imposed in the y-direction. Such measurements were beyond the scope of these experiments. However, some of these measurements have been made in the direct numerical simulations of O&P. They show that $\rho_{\partial v/\partial y,\,\partial\theta/\partial y}$ varies from -0.295 to -0.085 as the Reynolds number (R_λ) increases from 28 to 185. Over this same range, $\rho_{\partial u/\partial x,\,\partial\theta/\partial y}$ falls from 0.144 to 0.043. Since both correlation coefficients are tending towards zero – their locally isotropic values – it would appear that such statistics are not inheriting the anisotropy of the scalar field.

The correlation between $\partial v/\partial x$ and $\partial\theta/\partial x$ (or more generally between $\partial u_i/\partial x_k$ and $\partial\theta/\partial x_k$) is of particular physical interest since it is a component of the term representing the dissipation of turbulent heat flux $\langle\epsilon_{u_i\theta}\rangle$ in the heat flux budget (e.g. Townsend 1976):

$$\partial_t\langle\theta u_i\rangle + \langle U_k\rangle\partial_{x_k}\langle\theta u_i\rangle + \partial_{x_k}\langle\theta u_i u_k\rangle = -\langle u_i u_k\rangle\partial_{x_k}\langle T\rangle - \langle\theta u_k\rangle\partial_{x_k}\langle U_i\rangle$$
$$-\frac{1}{\rho}\langle\theta\partial_{x_i}p\rangle + \frac{g_i}{\langle T\rangle}\langle\theta^2\rangle + \partial_{x_k}(\kappa\langle u_i\partial_{x_k}\theta\rangle + \nu\langle\theta\partial_{x_k}u_i\rangle) - (\nu+\kappa)\langle\partial_{x_k}u_i\partial_{x_k}\theta\rangle. \quad (3.5)$$

For a steady, quasi-homogeneous flow (i.e. neglecting all inhomogeneitites except for the decay of the turbulence) with no mean velocity gradients, one can write a simplified form of the above equation for the heat flux in the direction of the mean gradient (i.e. the y-direction):

$$\langle U\rangle\partial_x\langle\theta v\rangle = -\langle v^2\rangle\beta - \frac{1}{\rho}\langle\theta\partial_y p\rangle + \frac{g}{\langle T\rangle}\langle\theta^2\rangle - (\nu+\kappa)\langle\partial_{x_k}v\partial_{x_k}\theta\rangle. \quad (3.6)$$

The correlation coefficient defined in equation (3.4) is related to one of the three components of the dissipation of turbulent heat flux $\langle\epsilon_{v\theta}\rangle$ (the last term in equation (3.6)). By local isotropy arguments, is often assumed that $\langle\epsilon_{v\theta}\rangle$ is zero in flows with large enough Reynolds numbers. (The production of heat flux is then balanced by the pressure-scrambling term.) To test the validity of this assumption, we follow O&P by plotting in figure 9 the ratio of (one-component of) the dissipation of (transverse) turbulent heat flux to its production, $-\langle v^2\rangle\beta$. It is emphasized that the numerator only represents one of the three components of the total dissipation of transverse turbulent

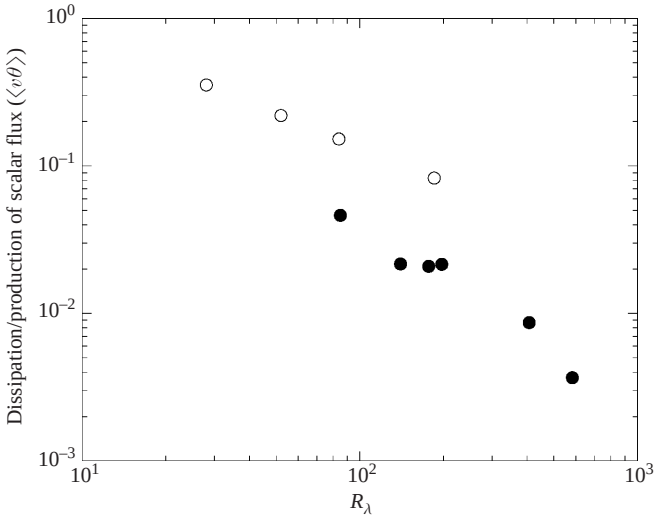

FIGURE 9. The ratio of the dissipation of turbulent heat flux, $\langle \epsilon_{v\theta} \rangle$, to its production: ●, $(\nu + \kappa)\langle(\partial v/\partial x)(\partial\theta/\partial x)\rangle/(-\langle v^2\rangle\beta)$ – present work; ○, $\langle \epsilon_{v\theta} \rangle/(-\langle v^2\rangle\beta) = (\nu + \kappa)\langle(\partial v/\partial x_i)(\partial\theta/\partial x_i)\rangle/(-\langle v^2\rangle\beta)$ – DNS of O&P.

heat flux. Also plotted in figure 9 is the ratio of the total dissipation of transverse turbulent heat flux to its production, as determined by O&P. Both sets of data tend to zero as the Reynolds number is increased. As would be expected, the two sets of data have different values, with the data of O&P (for the complete dissipation, $\langle \epsilon_{v\theta} \rangle$) being larger by a factor of approximately 3 to 4. However, the Reynolds number dependence for both sets of data is similar and the present data roughly follow an $R_\lambda^{-1.2}$ power law. (The data of O&P follow an $R_\lambda^{-0.77}$ power law.)

We next discuss third-order mixed derivative statistics. In particular, we consider non-dimensional, skewness-like statistics, $S_\alpha(m, n)$, where

$$S_\alpha(m, n) = \frac{\langle(\partial_x u_\alpha)^m(\partial_x\theta)^n\rangle}{(\partial_x u_\alpha)^m_{rms}(\partial_x\theta)^n_{rms}}. \tag{3.7}$$

(For these to be considered 'skewnesses', $m + n$ must equal 3.) In figure 10, $S_1(1, 2)$, $S_1(2, 1)$, $S_2(1, 2)$ and $S_2(2, 1)$ are plotted as a function of Reynolds number. In an isotropic flow, $S_1(2, 1)$, $S_2(1, 2)$ and $S_2(2, 1)$ must be zero. This is indeed the case to within the experimental scatter. The term $\langle(\partial_x u)(\partial_x\theta)^2\rangle$ (i.e. the numerator of $S_1(1, 2)$) represents the production of $\langle(\partial_x\theta)^2\rangle$ by stretching of the temperature field resulting from the action of the turbulent strain field (Wyngaard 1971). Over the range of Reynolds numbers considered in this paper, $S_1(1, 2) \approx -0.4 \pm 0.1$. Such a result is consistent with previous measurements (see Sreenivasan & Antonia (1997) for a compilation of laboratory and atmospheric data) and numerical simulations (e.g. Wang, Chen & Brasseur 1999). Antonia & Chambers (1980), using arguments put forth by Van Atta (1974), predict that the Reynolds number dependence of $S_1(1, 2)$ should be weak (i.e. $R_\lambda^{0.0375}$ or $R_\lambda^{0.15}$, depending on the estimates of the scalar intermittency exponent, μ_θ, and the correlation coefficient between $\ln(\epsilon)$ and $\ln(\epsilon_\theta)$). Though the compilation of Sreenivasan & Antonia (1997) displays an $R_\lambda^{\sim 0.15}$ dependence of $S_1(1, 2)$, in this work such a weak Reynolds number dependence is indiscernible from the experimental scatter over our smaller Reynolds number range that does not include atmospheric flows.

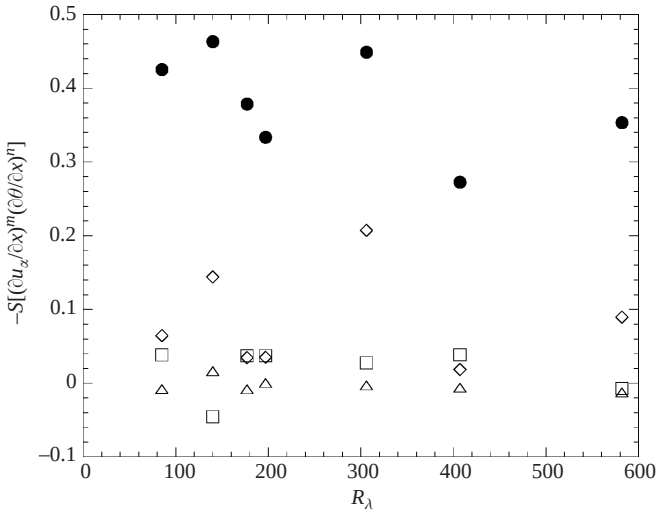

FIGURE 10. Mixed derivative skewnesses as a function of Reynolds number: ●, $S_1(1,2)$; □, $S_2(1,2)$; ◇, $S_1(2,1)$; △, $S_2(2,1)$. See equation (3.7) for definitions.

At the fourth order, we can consider kurtosis-like statistics. We define K_α as

$$K_\alpha = \frac{\langle(\partial_x u_\alpha)^2(\partial_x\theta)^2\rangle}{(\partial_x u_\alpha)^2_{rms}(\partial_x\theta)^2_{rms}}. \tag{3.8}$$

K_1 and K_2 are both 2.0 ± 0.5 and show no discernible Reynolds number dependence. They are not measures of the internal intermittency of the scalar field. Rather, these are measures of the correlation between the dissipation of turbulent kinetic energy, ϵ, and the dissipation of the scalar variance, ϵ_θ. It can be shown that

$$K = 1 + \rho_{\epsilon,\epsilon_\theta}\frac{\epsilon_{rms}}{\langle\epsilon\rangle}\frac{\epsilon_{\theta rms}}{\langle\epsilon_\theta\rangle}, \tag{3.9}$$

where the formal correlation coefficient between ϵ and ϵ_θ, $\rho_{\epsilon,\epsilon_\theta}$, is given by

$$\rho_{\epsilon,\epsilon_\theta} \equiv \frac{\langle(\epsilon - \langle\epsilon\rangle)(\epsilon_\theta - \langle\epsilon_\theta\rangle)\rangle}{\epsilon_{rms}\epsilon_{\theta rms}}. \tag{3.10}$$

Therefore, the $O(1)$ value of K_1 and K_2 implies a low correlation between ϵ and ϵ_θ, given that the 'dissipation intensities', $\epsilon_{rms}/\langle\epsilon\rangle$ and $\epsilon_{\theta rms}/\langle\epsilon_\theta\rangle$, are approximately 3 and 4.5, respectively.† This is explicitly observed in figure 11, where the correlation coefficient between ϵ and ϵ_θ is plotted and found to be $O(0.1)$ and decreasing with Reynolds number. Included in figure 11 are the data of O&P who calculate $\rho_{\epsilon,\epsilon_\theta}$ using the total definitions of ϵ (or the pseudo-dissipation, $\epsilon_p \equiv \nu(\partial u_i/\partial x_j)(\partial u_i/\partial x_j)$) and ϵ_θ. It is emphasized that, for the present data, the dissipations are estimated by their one-dimensional surrogates: $\epsilon = \epsilon^{11} = 15\nu\langle U\rangle^{-2}(\partial u/\partial t)^2$ or $\epsilon = \epsilon^{21} = 7.5\nu\langle U\rangle^{-2}(\partial v/\partial t)^2$ and $\epsilon_\theta = \epsilon^{\theta 1} = 3.4\kappa\langle U\rangle^{-2}(\partial\theta/\partial t)^2$. The data for $\rho_{\epsilon_p,\epsilon_\theta}$ from O&P are in slightly better agreement with the present (surrogate-based) data than their data for $\rho_{\epsilon,\epsilon_\theta}$. This is to be expected since ϵ_p more closely resembles the surrogates used herein – neither include the cross-terms, $(\partial u_i/\partial x_j)(\partial u_j/\partial x_i)$, present in the total definition of the dissipation of turbulent kinetic energy.

† More precisely, as R_λ increases from 85 to 582, $\epsilon^{11}_{rms}/\langle\epsilon^{11}\rangle$ increases from 2.3 to 2.9, $\epsilon^{21}_{rms}/\langle\epsilon^{21}\rangle$ increases from 2.7 to 3.4 while $\epsilon^{\theta 1}_{rms}/\langle\epsilon^{\theta 1}\rangle$ falls between 3.9 and 5.1. Both $\epsilon^{11}_{rms}/\langle\epsilon^{11}\rangle$ and $\epsilon^{21}_{rms}/\langle\epsilon^{21}\rangle$ show clear $R_\lambda^{\sim 0.1}$ Reynolds number dependences while no such a dependence can be distinguished from the scatter in $\epsilon^{\theta 1}_{rms}/\langle\epsilon^{\theta 1}\rangle$.

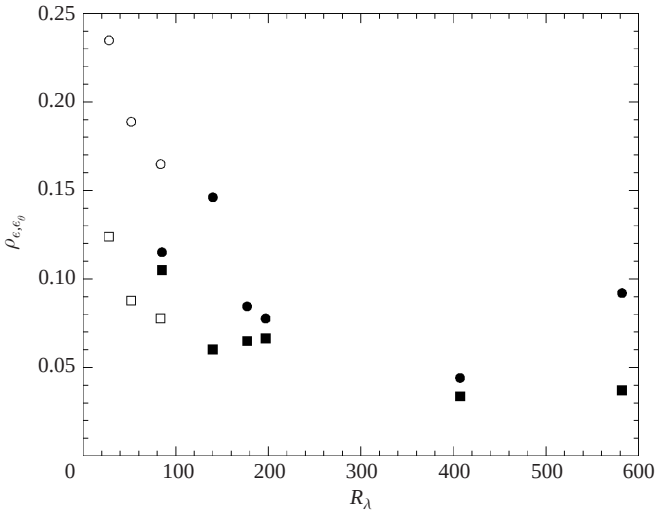

FIGURE 11. The correlation coefficient between ϵ and ϵ_θ as a function of Reynolds number. Solid symbols represent the present work. Open symbols represent the DNS of O&P. ●, $\rho_{\epsilon^{11},\epsilon^{\theta 1}}$; ■, $\rho_{\epsilon^{21},\epsilon^{\theta 1}}$; ○, $\rho_{\epsilon,\epsilon_\theta} = \rho_{13}$ of O&P; □, $\rho_{\epsilon_p,\epsilon_\theta} = \rho_{14}$ of O&P.

To determine the effect of internal intermittency on the mixed velocity–passive scalar field, we calculate PDFs of $\Delta v(r)\Delta\theta(r)$ for various separations, r, that extend from $r/\eta \sim 2.5$ to $r/\ell \sim 0.5$. These are shown for two Reynolds numbers ($R_\lambda = 85$ and 407) in figures 12(a) and 12(b), respectively. In the limit $r \to 0$, these become the PDFs of $(\partial v/\partial x)(\partial\theta/\partial x)$. In the limit $r \to \infty$, the PDFs tend towards the PDFs of the turbulent heat flux, $v\theta$. As the separation, r, is reduced, the tails of the PDF broaden, reflecting the increased probability of rare events many standard deviations away from the mean. The tails of the PDFs also change from being approximately exponential at large separations (i.e. figure 2) to being super-exponential at the smallest scales.

We also observe that the (negative) skewness of the PDF of $\Delta v\Delta\theta$ for the smallest separations decreases with Reynolds number. At large scales, the imposed gradient induces a skewness in the PDF of $\Delta v\Delta\theta$, independent of Reynolds number. However, for large separation of scales (i.e. large Reynolds numbers), the anisotropy generated by the mean temperature gradient is not communicated to the smallest scales.

The kurtosis of $(\partial v/\partial x)(\partial\theta/\partial x)$ is 225 ± 75. There is significant scatter since this is an eighth-order derivative statistic.

3.4. *The conditional statistics*

Conditional statistics of mixed velocity–passive scalar statistics are of particular interest to turbulence theoreticians and modellers, particularly due to their appearance in the governing equation for the PDF of a passive scalar. The evolution equation for the one-point, one-time Eulerian PDF of the scalar fluctuation, $f_\theta(\psi; x_i, t)$, is (Pope 2000)

$$\frac{\partial f_\theta}{\partial t} + \frac{\partial}{\partial x_i}[f_\theta(\langle U_i\rangle + \langle u_i|\psi\rangle)] = -\frac{\partial}{\partial\psi}\left(f_\theta\left\langle \frac{\mathrm{D}\theta}{\mathrm{D}t}\middle|\psi\right\rangle\right)$$
$$= -\frac{\partial}{\partial\psi}(f_\theta[\langle\kappa\nabla^2\theta|\psi\rangle + \langle S(\theta)|\psi\rangle]), \qquad (3.11)$$

where ψ is the sample-space variable representing θ. We remark that $\langle u_i|\psi\rangle$ denotes $\langle u_i(x_i,t)|\theta(x_i,t) = \psi\rangle$. (Similar notation is used for the other conditional expectations.)

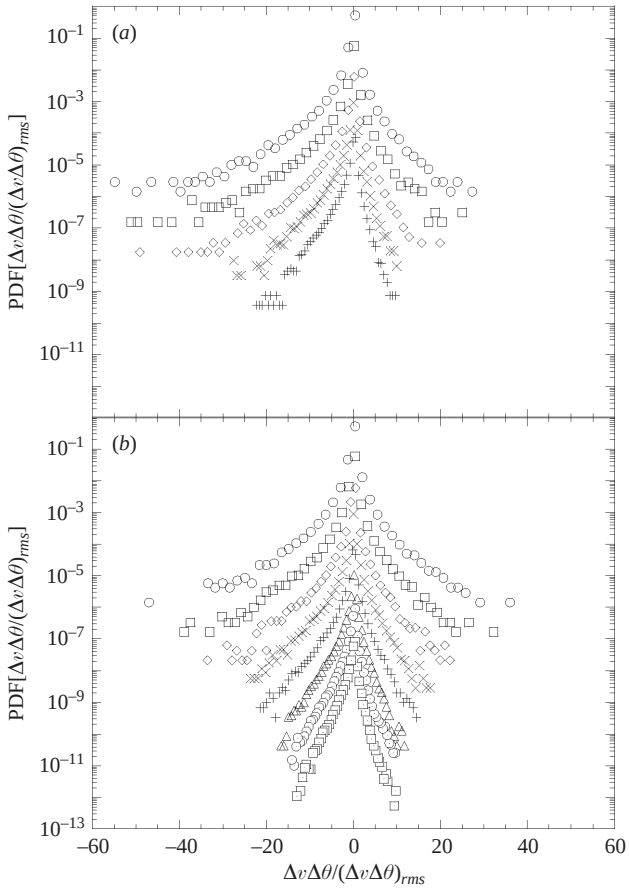

FIGURE 12. Probability density functions of $\Delta v(r)\Delta\theta(r)$ for various separations, r, extending from $r/\eta \sim 2.5$ to $r/\ell \sim 0.5$. (*a*) $R_\lambda = 85$: ○, $r/\eta = 2.3$; □, $r/\eta = 4.6$; ◇, $r/\eta = 11.6$; ×, $r/\eta = 25.5$; +, $r/\eta = 51.0$. (*b*) $R_\lambda = 407$: ○, $r/\eta = 2.8$; □, $r/\eta = 5.7$; ◇, $r/\eta = 11.3$; ×, $r/\eta = 22.7$; +, $r/\eta = 48.2$; △, $r/\eta = 99.1$; ⊙, $r/\eta = 198$; ⊡, $r/\eta = 397$.

$S(\theta)$ is the source term, which, in the present flow, is equal to $-u_i\partial\langle T\rangle/\partial x_i = -v\beta$ (i.e. production of scalar fluctuations by the mean scalar gradient). The above equation can also be re-written in the following manner (Pope 2000):

$$\frac{\overline{\mathrm{D}}f_\theta}{\overline{\mathrm{D}}t} = \kappa\nabla^2 f_\theta - \frac{\partial}{\partial x_i}(f_\theta\langle u_i|\psi\rangle) - \frac{\partial^2}{\partial\psi^2}\left(f_\theta\left\langle \kappa\frac{\partial\theta}{\partial x_i}\frac{\partial\theta}{\partial x_i}\middle|\psi\right\rangle\right) - \frac{\partial}{\partial\psi}[f_\theta\langle S(\theta)|\psi\rangle]. \quad (3.12)$$

In these equations, the effects of the turbulent convective flux and molecular diffusion are not in closed form and therefore require modelling.

More generally, the evolution equation for the one-point, one-time joint Eulerian PDF of the velocity and the scalar, $f_{u_i\theta}(V_i,\psi;x_i,t)$, is also of interest. Its governing equation, deduced from the Navier–Stokes and the advection–diffusion equations, is (Pope 2000)

$$\frac{\partial f_{u_i\theta}}{\partial t} + V_i\frac{\partial f_{u_i\theta}}{\partial x_i} - \frac{1}{\rho}\frac{\partial\langle p\rangle}{\partial x_i}\frac{\partial f_{u_i\theta}}{\partial V_i} + \frac{\partial}{\partial\psi}[f_{u_i\theta}\langle S(\theta)|\psi\rangle]$$
$$= -\frac{\partial}{\partial V_i}\left(f_{u_i\theta}\left\langle \nu\nabla^2 U_i - \frac{1}{\rho}\frac{\partial p'}{\partial x_i}\middle| V_i,\psi\right\rangle\right) - \frac{\partial}{\partial\psi}[f_{u_i\theta}\langle\kappa\nabla^2\theta|V_i,\psi\rangle], \quad (3.13)$$

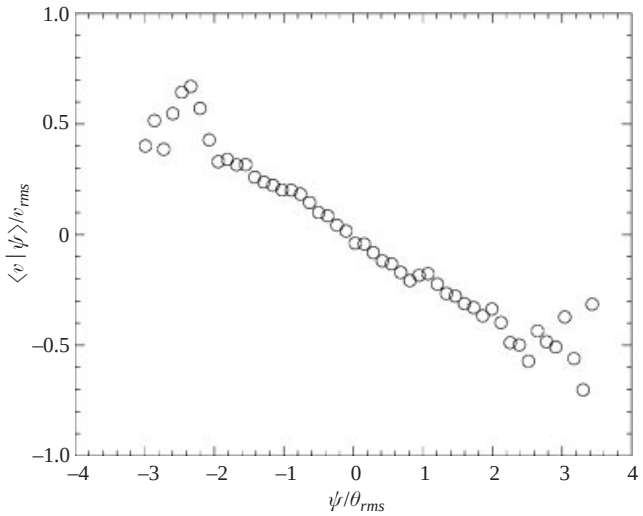

FIGURE 13. A typical expectation of the transverse velocity fluctuation conditioned on the scalar fluctuation. $R_\lambda = 582$.

where V_i is the sample-space variable representing the instantaneous velocity, U_i. From the above equation, it can be seen that the joint conditional Laplacian of the scalar ($\langle\nabla^2\theta|V_i,\psi\rangle$) must be modelled. However, because $f_{u_i\theta}$ contains information on the velocity field, turbulent convection appears in closed form and does not require modelling.

In this section, we will therefore examine $\langle u_i|\psi\rangle$, $\langle\nabla^2\theta|V_i\rangle$ and $\langle\nabla^2\theta|V_i,\psi\rangle$. (The other mixed velocity–passive scalar conditional expectation in equation (3.13), $\langle\nabla^2 U_i|\psi\rangle$, should be zero since the velocity is independent of the scalar due to the latter's passive nature. This was indeed verified, but is not shown here.)

The conditional expectations $\langle\nabla^2\theta|\psi\rangle$ and $\langle\epsilon_\theta|\psi\rangle$ (i.e. the conditional Laplacian of the scalar and the conditional scalar dissipation) describe the effects of molecular diffusion. These are not mixed velocity–passive scalar statistics *per se*, but are of interest and are therefore discussed in Appendix B.

A typical plot of the expectation of the transverse velocity fluctuation (i.e. the fluctuation in the direction of the mean scalar gradient) conditioned on the scalar fluctuation, $\langle v|\psi\rangle$, is shown in figure 13 at $R_\lambda = 582$. The conditional expectation is approximately linear with negative slope. Similar results were also obtained by O&P and Venkataramani & Chevray (1978). Given a linear conditional expectation, it can be proven that the slope of the curve must be equal to the correlation coefficient between the two variables. (Furthermore, a linear conditional expectation is obtained when two variables are jointly Gaussian. This is not exactly the case here, but is a reasonable approximation at large scales.) The expectations of the transverse velocity conditioned on the scalar value were approximately linear for all Reynolds numbers and exhibited no significant Reynolds number dependence. The only variation was in their slope, which results from the previously discussed changes in the correlation between v and θ.

In contrast to the previous figure, a significant Reynolds number dependence is observed in figure 14, where the conditional expectation $\langle\partial^2\theta/\partial x^2|V\rangle$ is shown (with $V = V_2$); $\langle\partial^2\theta/\partial x^2|V\rangle$ is a surrogate for the total Laplacian of the scalar, $\langle\nabla^2\theta|V\rangle$, which has three components. As shown in Pope (1998), Taylor's (1921) hypothesis of

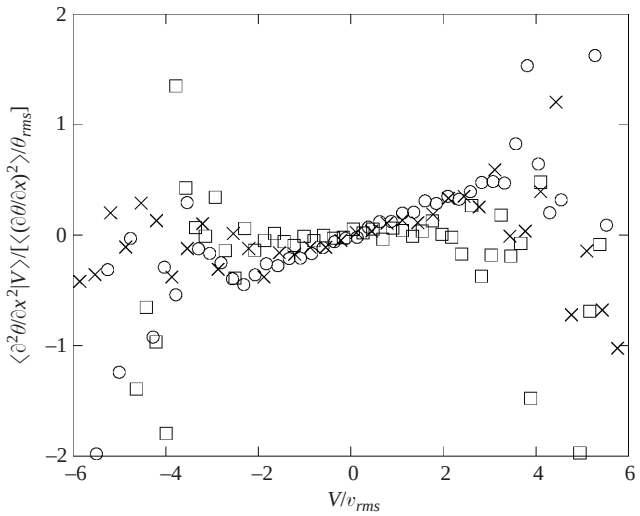

FIGURE 14. The expectation of $\partial^2\theta/\partial x^2$ conditioned on the transverse velocity fluctuation: ○, $R_\lambda = 85$; ×, $R_\lambda = 197$; □, $R_\lambda = 582$.

diffusivity independence implies

$$\lim_{Re,Pe\to\infty}\left\{\frac{\theta_{rms}\langle\nabla^2\theta|V_i\rangle}{\langle\nabla\theta\cdot\nabla\theta\rangle}\right\} = \lim_{Re,Pe\to\infty}\left\{\frac{\kappa\theta_{rms}\langle\nabla^2\theta|V_i\rangle}{\langle\epsilon_\theta\rangle}\right\} = 0. \tag{3.14}$$

Local isotropy does not imply that $\langle\nabla^2\theta|V_i\rangle$ is zero. However, local isotropy in conjunction with $\langle\nabla^2\theta|V_i\rangle$ being an odd function of u_i implies that $\langle\nabla^2\theta|V_i\rangle$ must be zero (Pope 1998). As can be seen in figure 14, (the surrogate of) $\langle\nabla^2\theta|V\rangle$ is approximately linear in v and passes through the origin. It should therefore tend to zero in a locally isotropic flow. This is observed to be the case. At $R_\lambda = 85$, the slope of (the central, better-converged portion of) this curve is 0.17, consistent with the results of O&P. At $R_\lambda = 197$, the slope of the curve is 0.13 and at $R_\lambda = 582$, the slope is 0.03 – effectively zero. The scalar mixing term is not independent of the velocity for lower Reynolds numbers. This anisotropy must therefore be included in models of this conditional expectation. Consequently, a velocity-conditioned model of $\langle\nabla^2\theta|V_i\rangle$ and $\langle\nabla^2\theta|V_i,\psi\rangle$ has been put forth by Fox (1996).

We make two last points regarding $\langle\partial^2\theta/\partial x^2|V\rangle$. First, a surrogate of $\nabla^2\theta$ was used. It would be of particular interest to consider the other two terms ($\partial^2\theta/\partial y^2$ and $\partial^2\theta/\partial z^2$) in $\nabla^2\theta$. The behaviour of $\langle\partial^2\theta/\partial y^2|V\rangle$ would be of particular interest given that the derivative is in the direction of the mean scalar gradient. Secondly, $\langle\partial^2\theta/\partial x^2|V\rangle$ was non-dimensionalized by $\langle(\partial\theta/\partial x)^2\rangle/\theta_{rms}$. Non-dimensionalization by $(\partial^2\theta/\partial x^2)_{rms}$ is also possible. This latter non-dimensionalization was not chosen since $(\partial^2\theta/\partial x^2)_{rms}/[\langle(\partial\theta/\partial x)^2\rangle/\theta_{rms}]$ scales as $R_\lambda^{1/2}$. Such a spurious R_λ-dependence interferes with the verification of equation (3.14).

The last statistic to be discussed in this section is the expectation of the Laplacian of the scalar jointly conditioned on the velocity and scalar fluctuations, $\langle\nabla^2\theta|V_i,\psi\rangle$. $\langle\nabla^2\theta|V_i\rangle$ was discussed above and $\langle\nabla^2\theta|\psi\rangle$ is discussed in Appendix B, where no Reynolds number dependence is observed. In figures 15(a) and 15(b), the surrogate of $\langle\nabla^2\theta|V_i,\psi\rangle$, $\langle\partial^2\theta/\partial x^2|V,\psi\rangle$, is respectively shown for two Reynolds numbers, $R_\lambda = 85$ and $R_\lambda = 582$. Two observations can be made. The first is that the shape of the conditional expectation changes from ellipsoidal towards circular. This results from

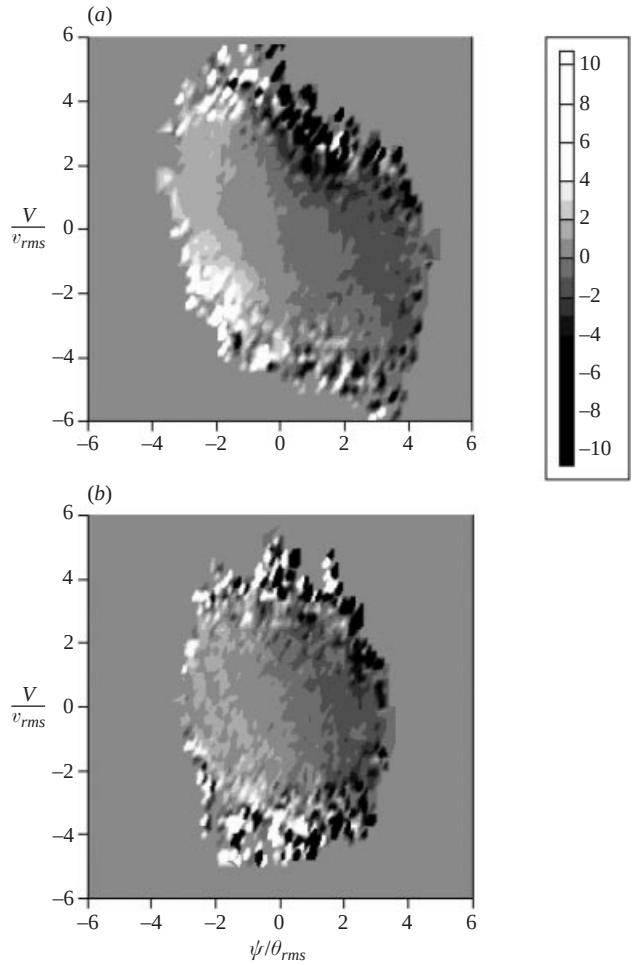

FIGURE 15. The expectation of $\partial^2\theta/\partial x^2$ (normalized by $\langle(\partial\theta/\partial x)^2\rangle/\theta_{rms}$) jointly conditioned on the transverse velocity and scalar fluctuations. (*a*) $R_\lambda = 85$; (*b*) $R_\lambda = 582$.

the aforementioned changing correlation coefficient between v and θ. The second observation is the change in the slope of lines of constant $\partial^2\theta/\partial x^2$. At low Reynolds numbers, these are negatively sloped. At high Reynolds numbers, the lines become vertical. The latter effect results from the diminishing influence of the velocity on scalar mixing as the Reynolds number increases. This same effect is what renders the conditional expectations of $\langle\partial^2\theta/\partial x^2|V\rangle$ flat in the limit of large R_λ in figure 14. Note that the (extreme) white and black zones that are close to each other are not significant. These regions are multiple standard deviations away from the mean and contain very few data points. Therefore, the value of $\partial^2\theta/\partial x^2$ in these zones has yet to converge.

4. Conclusions

The evolution with Reynolds number of mixed velocity–passive scalar statistics was studied over the range $85 \leqslant R_\lambda \leqslant 582$ in decaying grid turbulence with an imposed mean scalar gradient. The PDFs of the turbulent heat flux, $v\theta$, exhibited exponential tails, consistent with the quasi-joint-Gaussian nature of the mixed velocity–passive

scalar statistics. The turbulent Nusselt number continually increased with Reynolds number. However, the rate at which it did so was influenced by the value of the correlation coefficient, $\rho_{v\theta}$. For the Reynolds numbers considered, the ratio of the mechanical to thermal time scale, R, was 1.28 ± 0.07, roughly independent of Reynolds number.

The mixed velocity–passive scalar co-spectra and structure functions developed slowly, resembling more closely the velocity field than the scalar field. The inertial-range scaling exponents (at the second order) were still significantly below the Kolmogorovian (in the 1941 sense) predictions for the largest Reynolds numbers. In this limit, the heat flux co-spectrum inertial-range scaling exponent was ~ -2.0, significantly different from the theoretical prediction of $-7/3$. The inertial-range scaling exponent of the heat flux structure structure functions, $\langle \Delta v \Delta\theta \rangle$, was ~ 1.0 – less than the corresponding prediction of $4/3$. The behaviour of the sixth-order longitudinal mixed structure function, $\langle (\Delta u)^2 (\Delta\theta)^4 \rangle$, exhibited inertial-range scaling exponents of 1.36–1.52 (or 1.55–1.67 when estimated by means of ESS). Though in approximate agreement with the few other existing measurements of $\langle (\Delta u)^2 (\Delta\theta)^4 \rangle$, the discrepancies can most likely be attributed to (i) the different methods for determining the scaling exponents, (ii) the effect of shear on the scalar field, and (iii) the repercussions of mean scalar gradients, decay of the turbulence, etc. on the behaviour of $\langle (\Delta u)^2 (\Delta\theta)^4 \rangle$.

All fine-scale statistics behaved in a manner consistent with local isotropy. That is, quantities that should be zero in a locally isotropic flow – such as the correlation coefficient between $\partial v/\partial x$ and $\partial\theta/\partial x$, $\rho_{\partial v/\partial x, \partial\theta/\partial x}$, the dissipation of $v\theta$, $\langle \epsilon_{v\theta} \rangle$ – were so, or decayed towards zero as the Reynolds number was increased. However, we emphasize that for the assumption of local isotropy of the mixed velocity–scalar field to be valid requires, for the measured fine-scale statistics studied herein, at least $R_\lambda > 200$. At high Reynolds numbers, the PDFs of $\Delta v \Delta\theta$ lost their asymmetry at small scales (as required by local isotropy) and their tails broadened (reflecting the effect of internal intermittency on the mixed velocity–passive scalar field).

Three mixed velocity–passive scalar conditional expectations (of immediate interest to PDF modellers) were studied. An approximately linear behaviour of $\langle v|\psi \rangle$ (with slope equal to $\rho_{v\theta}$) independent of Reynolds number was observed. In contrast, $\langle \partial^2\theta/\partial x^2 | V_i \rangle$ exhibited a linear behaviour with a slope that tended towards zero in the limit of large Reynolds numbers. This result validates the diffusivity independence hypothesis (Taylor 1921; Pope 1998) and is also exhibited in the joint conditional expectation $\langle \nabla^2\theta | V_i, \psi \rangle$. The effect of the imposed anisotropy is observed up to significant Reynolds numbers (i.e. $R_\lambda \sim 500$) and, to be accounted for in models, requires consideration of the joint PDF of the velocity and the scalar.

It is re-emphasized that other statistics should be studied before local isotropy of the mixed velocity–passive scalar field can be completely validated. Measurements that include temperature differences or derivatives in the direction of the mean gradient are required. Some statistics of this type were estimated in the direct numerical simulations of Overholt & Pope (1996) and tended towards zero as the Reynolds number was increased.

We also point out that no large-scale anisotropy was present in the velocity field studied herein. The velocity field in homogeneous shear flow has been shown to exhibit anisotropies (Shen & Warhaft 2000; Ferchichi & Tavoularis 2000; Warhaft & Shen 2001), though less prominent than those observed in the scalar field. It would therefore also be of interest to determine whether such velocity field anisotropies contaminate the mixed field – particularly since the mixed statistics more closely resemble those of the velocity than the scalar in their evolution.

The author would like to thank Professor Z. Warhaft for beneficial discussions. Dr G. Xu and Professor R. A. Antonia are also thanked for kindly supplying their data for use in figure 7. Lastly, the referees are thanked for offering some constructive comments. Support has been provided by the Natural Sciences and Engineering Research Council of Canada and the Fonds pour la Formation de Chercheurs et l'Aide à la Recherche du Québec. The measurements were made at Cornell University by means of support from the United States Department of Energy (Basic Energy Sciences).

Appendix A. Comparison of the scaling exponents of $\langle(\Delta u)^2(\Delta\theta)^4\rangle$ with model predictions

It is of interest to compare the scaling exponent of $\langle(\Delta u)^2(\Delta\theta)^4\rangle$ for our highest Reynolds number ($R_\lambda = 582$) with the prediction of two models. The first model, suggested by Xu *et al.* (2000*a*), assumes a bivariate, joint-lognormal distribution between ϵ_r and ϵ_{θ_r} (where the subscript r indicates averaging over a sphere of radius r, which we approximate by averaging over a linear distance r). Making this assumption, one obtains (Xu *et al.* 2000*a*)

$$\zeta_{u\theta}(m,n) = \zeta_u(m) + \zeta_\theta(n) + \frac{\mu^{1/2}}{18}(\mu^{1/2} - 3\rho\mu_\theta^{1/2})mn, \tag{A 1}$$

where $\zeta_u(m)$ is the scaling exponent of the mth-order velocity structure function, $\zeta_\theta(n)$ is the scaling exponent of the nth-order scalar structure function, $\zeta_{u\theta}(m,n)$ is the scaling exponent of the $(m+n)$th-order mixed mth-order velocity/nth-order scalar structure function, ρ is the centred correlation coefficient between $\ln(\epsilon_r)$ and $\ln(\epsilon_{\theta_r})$, μ is the velocity intermittency exponent and μ_θ, as already mentioned, is the scalar intermittency exponent.

Before proceeding, we briefly digress and discuss the intermittency exponents. At $R_\lambda = 582$, μ and μ_θ were determined to be 0.12 and 0.25 respectively (from the non-centred autocorrelations of the dissipations – see M&W96 and M&W98). (μ was found to be a strong function of the Reynolds number in M&W96 and, in the limit of high Reynolds number, is thought to be 0.25 ± 0.05 (Sreenivasan & Kailasnath 1993).) The value of μ_θ has not received the same amount of attention. Estimates of μ_θ vary from 0.17 (Xu *et al.* 2000*a*), to 0.25 (e.g. M&W98, Chambers & Antonia 1984) to 0.35 (e.g. Prasad, Meneveau & Sreenivasan 1988; Sreenivasan, Antonia & Danh 1977). We remark that the value of μ_θ obtained in M&W98 (0.25) is not consistent with the value obtained from the sixth-order longitudinal mixed structure function at $R_\lambda = 582$ (i.e. $\mu_\theta = 2 - \zeta_{u\theta}(2,4) = 2 - 1.52 = 0.48$). This discrepancy may arise from the various methods by which μ_θ (or μ) can be estimated. The different approaches to the calculation of μ were discussed in Sreenivasan & Kailasnath (1993). Some of these methods become equivalent in the limit of high Reynolds number. Since the velocity field has not yet reached its high-Reynolds-number limit by $R_\lambda \sim 600$ (M&W96), this may perhaps explain the discrepancy. However, as with $\langle(\Delta u)^2(\Delta\theta)^4\rangle$, this requires further study.

In addition, μ_θ, as determined from $\langle(\Delta u)^2(\Delta\theta)^4\rangle$, may differ from other estimates of μ_θ due to the effects of (i) decay of the turbulence and (ii) turbulent production of temperature fluctuations. In Danaila *et al.* (1999) and Danaila & Mydlarski (2001), respectively, it was shown that both these phenomena had a significant effect on $\langle\Delta u(\Delta\theta)^2\rangle$. It was these effects that caused inertial-range deviations of $\langle\Delta u(\Delta\theta)^2\rangle$ from Yaglom's (1949) prediction of $-(4/3)\langle\epsilon_\theta\rangle r$; the smaller the Reynolds number, the

larger the deviation. For very low Reynolds numbers (i.e. $R_\lambda < 50$), the deviation even penetrated into the dissipative range. There is no reason to expect that the same two phenomena are not affecting $\langle(\Delta u)^2(\Delta\theta)^4\rangle$, and thus the determination of μ_θ from the structure function. What is unclear, however, is if and how the decay and production affect estimates of μ_θ as estimated by other methods, such as the autocorrelation of the dissipation. The effect could be equivalent, but this has yet to be shown.

We now return to the calculation of $\zeta_{u\theta}(2,4)$ by means of equation (A 1). The value of ρ was estimated for two different inertial-range separations, r_a and r_b. These correspond to the middle of the inertial-range when the spectrum is plotted in linear and logarithmic coordinates, respectively. (This is explained in detail in M&W96. Note that $r_b > r_a$.) For ϵ determined from $\epsilon = 15\nu(\partial u/\partial x)^2$, $\rho = \rho_{ln(\epsilon_{r_a}),ln(\epsilon_{\theta_{r_a}})} = 0.22$ and $\rho = \rho_{ln(\epsilon_{r_b}),ln(\epsilon_{\theta_{r_b}})} = 0.17$. For ϵ determined from $\epsilon = 7.5\nu(\partial v/\partial x)^2$, $\rho = \rho_{ln(\epsilon_{r_a}),ln(\epsilon_{\theta_{r_a}})} = 0.20$ and $\rho = \rho_{ln(\epsilon_{r_b}),ln(\epsilon_{\theta_{r_b}})} = 0.13$. This agrees well with the results of Meneveau *et al.* (1990) ($\rho \approx 0.13$) and Xu *et al.* (2000*a*) ($\rho \approx 0.15$). Here we will use $\rho = 0.15$ (the average of the two estimates of ρ for the r_b separation. We choose the r_b separation since the scaling regions of the structure functions are studied in log–log coordinates – therefore r_b is the 'middle separation' in this case.) Using the values of μ and μ_θ from M&W98 (0.12 and 0.25, respectively) in conjunction with $\zeta_u(2) = 0.61$ and $\zeta_\theta(4) = 0.94$†, one obtains $\zeta_{u\theta}(2,4) = 1.57$ for $R_\lambda = 582$. This is close to our empirically determined value of $\zeta_{u\theta}(2,4) = 1.52$. (We remark that using $\mu = \mu_\theta = 0.25$ equation (A 1) predicts $\zeta_{u\theta}(2,4) = 1.61$.) The log-normal model therefore serves to validate the present estimates of $\zeta_{u\theta}(2,4)$ and reinforce our observation that $\zeta_{u\theta}(2,4) \neq 2 - \mu_\theta$, for μ_θ estimated from non-centred autocorrelations of ϵ_θ.

Similar results are obtained with the hierarchical structure model of Lévêque *et al.* (1999) (based on the analogous model of She & Lévêque (1994) for the velocity field). In their model, scaling exponents of $\langle \epsilon_{\theta_r}^p \rangle$ are expressed in terms of the scaling exponents of a hierarchy of fluctuation levels. The resulting model has two independent parameters – one is experimentally determined and the other is established from phenomenological arguments. The result is a prediction for Ψ_p, the scaling exponent of $\langle|(\Delta u(r))(\Delta\theta(r))^2|^{p/3}\rangle$:

$$\Psi_p = \frac{p}{9} + \frac{10}{9}\left(1 - \left(\frac{2}{5}\right)^{p/3}\right). \tag{A 2}$$

The prediction for Ψ_6 is 1.60 – a value close to the previous prediction of $\zeta_{u\theta}(2,4) = 1.57$ and our empirically determined value of 1.52. ($\zeta_{u\theta}(2,4)$, as defined by the model of Xu *et al.* (2000*a*), is equivalent to Ψ_6.)

Appendix B. Scalar conditional expectations

In equations (3.11) and (3.12), the conditional expectations $\langle\epsilon_\theta|\psi\rangle$ and $\langle\nabla^2\theta|\psi\rangle$, which describe the effects of molecular diffusion, appear. These are not mixed velocity–passive scalar statistics and are therefore discussed in this Appendix.

Measurements of the conditional scalar dissipation, $\langle\epsilon_\theta|\psi\rangle$, have been obtained by other authors (e.g. Jayesh & Warhaft 1992; Kailasnath, Sreenivasan & Saylor 1993; Anselmet, Djeridi & Fulachier 1994; Mi, Antonia & Anselmet 1995). In accordance

† $\zeta_u(2) = 0.69$ and $\zeta_\theta(4) = 1.03$ when determined by ESS conditioned on $|(\Delta u)^3|$ and $|\Delta u(\Delta\theta)^2|$, respectively. When these values are used, the prediction of the log-normal model is not as accurate as when directly determined exponents are used.

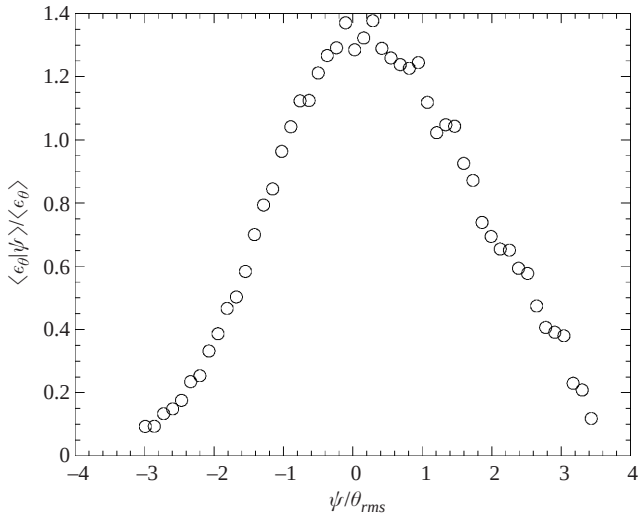

FIGURE 16. A typical expectation of the (surrogate of the) scalar dissipation rate conditioned on the scalar fluctuation. $R_\lambda = 582$.

with the theoretical results of Sinai & Yakhot (1989), O'Brien & Jiang (1991), Ching (1993) and Pope & Ching (1993), (i) a Gaussian PDF of the scalar is associated with ϵ_θ and θ being independent (e.g. Anselmet *et al.* 1994, figure 9*b*) and (ii) a super-Gaussian PDF of the scalar is associated with a rounded (concave-up) V-shape (e.g. Jayesh & Warhaft 1992). Jayesh & Warhaft (1992) noted that even though the underlying assumptions of self-similar flow with no mean gradient were not met, the results of Sinai & Yakhot (1989) compare well with the data. This was later explained by Pope & Ching (1993) who showed that a similar, and in one sense, more general, result to that of Sinai & Yakhot (1989) can be obtained by assuming a smooth stationary process (with a PDF decaying sufficiently rapidly for large fluctuations) and linearity of the conditional expectation of the second derivative of the aforementioned process. The latter assumption is equivalent to $\langle\nabla^2\theta|\psi\rangle$ being linear, if Taylor's hypothesis and local isotropy are valid. (In their derivation, Sinai & Yakhot (1989) assumed a homogeneous decaying field with no mean gradient that was governed by the advection–diffusion equation.) The agreement between the theoretical work of Sinai & Yakhot (1989) and the experiments of Jayesh & Warhaft (1992) was alternatively explained by Cai, O'Brien & Ladeinde (1996) and Sabel'nikov (1998), who extended the results of Sinai & Yakhot (1989) to the case of grid turbulence with an imposed mean scalar gradient. Here, the PDF of the scalar is shown to depend on the conditional scalar dissipation, $\langle\epsilon_\theta|\psi\rangle$, *and* the conditional expectation of the velocity fluctuation in the direction of the gradient, $\langle v|\psi\rangle$. It is shown that if the latter conditional expectation is linear (as was shown to approximately be the case in the present flow), then the PDF of the scalar does not explicitly depend on the mean scalar gradient. Linearity of $\langle v|\psi\rangle$ and $\langle\nabla^2\theta|\psi\rangle$ are related (see O&P or Sabel'nikov (1998)). Below, we will show that $\langle\partial^2\theta/\partial x^2|\psi\rangle$, a surrogate for $\langle\nabla^2\theta|\psi\rangle$, is also linear.

In the present work, where the PDF of the scalar is sub-Gaussian, the scalar dissipation (approximated by $(\partial\theta/\partial x)^2$) conditioned on the scalar has a concave-down, rounded V-shape, as shown in figure 16. (Such a result was typical for all Reynolds numbers. The peak of the curve is 1.3 ± 0.1 for all the Reynolds numbers.) Such a shape for $\langle\epsilon_\theta|\theta\rangle$ is consistent with the above-mentioned theoretical results and

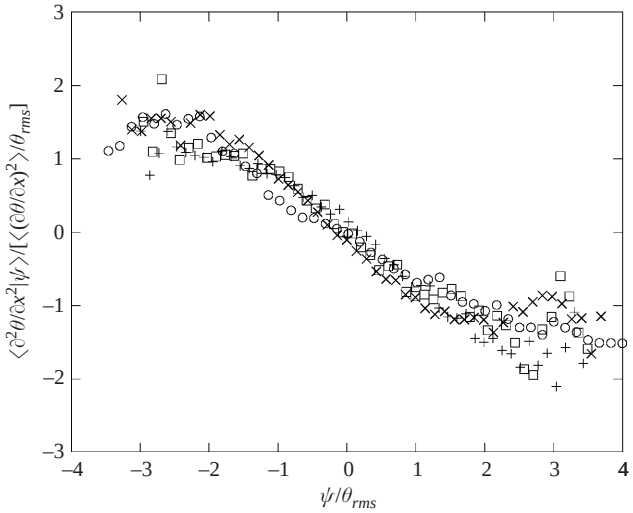

FIGURE 17. The expectation of $\partial^2\theta/\partial x^2$ conditioned on the temperature fluctuation: ○, $R_\lambda = 85$; ×, $R_\lambda = 197$; □, $R_\lambda = 407$; +, $R_\lambda = 582$.

a sub-Gaussian PDF of the scalar. The physical interpretation of this result is that large values of the scalar fluctuation are associated with low values of the scalar dissipation. This is in direct contrast with the work of Jayesh & Warhaft (1992). There, the ratio of the wind tunnel width to the integral length scale was much larger than for the present data. Thus, in the present work, the temperature fluctuations are bounded. Such a limitation in temperature results in low values of the scalar dissipation being associated with the extreme temperature fluctuations. One would expect a similar shape for $\langle\epsilon_\theta|\theta\rangle$ in a scalar mixing layer (e.g. Ma & Warhaft 1986). In such a flow, the scalar field is bounded by the temperatures of its two constituent streams. The resulting scalar PDF is also sub-Gaussian (Ma & Warhaft 1986).

Figure 17 presents the conditional expectation of $\partial^2\theta/\partial x^2$ on θ. It can be considered a surrogate for the Laplacian of the temperature field, $\nabla^2\theta$, conditioned on the scalar fluctuation, which appears in the equation for the scalar PDF. Like $\langle\epsilon_\theta|\psi\rangle$, $\langle\nabla^2\theta|\psi\rangle$ results from the effects of molecular diffusion. The conditional expectations in figure 17 are linear with negative slope in their inner region, where the data are better converged. There is no distinguishable Reynolds number dependence in the slopes of the conditional expectations. O&P observed a similar behaviour of $\langle\nabla^2\theta|\theta\rangle$.

REFERENCES

ANSELMET, F., DJERIDI, H. & FULACHIER, L. 1994 Joint statistics of a passive scalar and its dissipation in a turbulent jet. *J. Fluid Mech.* **280**, 173–197.

ANTONIA, R. A. & CHAMBERS, A. J. 1980 On the correlation between turbulent velocity and temperature derivatives in the atmospheric surface layer. *Boundary-Layer Met.* **18**, 399–410.

ANTONIA, R. A., HOPFINGER, E. J., GAGNE, Y. & ANSELMET, F. 1984 Temperature structure functions in turbulent shear flows. *Phys. Rev.* A **30**, 2704–2707.

ANTONIA, R. A. & VAN ATTA, C. W. 1978 Structure functions of temperature fluctuations in turbulent shear flows. *J. Fluid Mech.* **84**, 561–580.

BENZI, R., CILIBERTO, S., TRIPICCIONE, R., BAUDET, C., MASSAIOLI, F. & SUCCI, S. 1993 Extended self-similarity in turbulent flows. *Phys. Rev.* E **48**, R29–R32.

BORATAV, O. N. & PELZ, R. B. 1998 Coupling between anomalous velocity and passive scalar increments in turbulence. *Phys. Fluids* **10**, 2122–2124.

Browne, L. W. B., Antonia, R. A. & Chua, L. P. 1989 Calibration of X-probes for turbulent flow measurements. *Exps. Fluids* **7**, 201–208.

Cai, X. D., O'Brien, E. E. & Ladeinde, F. 1996 Uniform mean scalar gradient in grid turbulence: Asymptotic probability distribution of a passive scalar. *Phys. Fluids* **8**, 2555–2557.

Chambers, A. J. & Antonia, R. A. 1984 Atmospheric estimates of power law exponents μ and μ_θ. *Boundary-Layer Met.* **28**, 343–352.

Ching, E. S. C. 1993 Probability densities of turbulent temperature fluctuations. *Phys. Rev. Lett.* **70**, 283–286.

Corrsin, S. 1951 On the spectrum of isotropic temperature fluctuations in isotropic turbulence. *J. Appl. Phys.* **22**, 469–473.

Corrsin, S. 1952 Heat transfer in isotropic turbulence. *J. Appl. Phys.* **23**, 113–118.

Danaila, L., Anselmet, F., Zhou, T. & Antonia, R. A. 1999 A generalization of Yaglom's equation which accounts for the large-scale forcing in heated decaying turbulence. *J. Fluid Mech.* **391**, 359–372.

Danaila, L. & Mydlarski, L. 2001 Effect of gradient production on scalar fluctuations in decaying grid turbulence. *Phys. Rev.* E **64**, 0163161–0163169.

Ferchichi, M. & Tavoularis, S. 2000 Reynolds number effects on the fine structure of uniformly sheared turbulence. *Phys. Fluids* **12**, 2942–2953.

Fox, R. O. 1996 On velocity-conditioned scalar mixing in homogeneous turbulence. *Phys. Fluids* **8**, 2678–2691.

Garg, S. & Warhaft, Z. 1998 On the small-scale structure of simple shear flow. *Phys. Fluids* **10**, 662–673.

Gibson, C. H., Friehe, C. A. & McConnell, S. O. 1977 Skewness of temperature derivatives in turbulent shear flows. *Phys. Fluids Suppl.* **20**, s156–s167.

Haughdal, J. & Lienhard, V. H. 1988 A low cost high performance cold wire bridge. *J. Phys.* E **21**, 167–170.

Jayesh, Tong, C. & Warhaft, Z. 1994 On temperature spectra in grid turbulence. *Phys. Fluids* **6**, 306–312.

Jayesh & Warhaft, Z. 1992 Probability distribution, conditional dissipation, and transport of passive temperature fluctuations in grid generated turbulence. *Phys. Fluids* A **4**, 2292–2307.

Kailasnath, P., Sreenivasan, K. R. & Saylor, J. R. 1993 Conditional scalar dissipation rates in turbulent wakes, jets, and bounday layers. *Phys. Fluids* A **5**, 3207–3215.

Kolmogorov, A. N. 1941*a* The local structure of turbulence in incompressible viscous fluid for very large Reynolds numbers. *Dokl. Akad. Nauk. SSSR* **30**, 301–305.

Kolmogorov, A. N. 1941*b* Dissipation of energy in locally isotropic turbulence. *Dokl. Akad. Nauk. SSSR* **32**, 16–18.

Kolmogorov, A. N. 1962 A refinement of previous hypotheses concerning the local structure of turbulence in a viscous incompressible fluid at very high Reynolds numbers. *J. Fluid Mech.* **13**, 82–85.

Lévêque, E., Ruiz-Chavarria, G., Baudet, C. & Ciliberto, S. 1999 Scaling laws for the turbulent mixing of a passive scalar in the wake of a cylinder. *Phys. Fluids* **11**, 1869–1879.

Lienhard, J. H. 1988 The decay of turbulence in thermally stratified flow. PhD dissertation, University of California at San Diego.

Lienhard, J. H. & Van Atta, C. W. 1990 The decay of turbulence n thermally stratified flow. *J. Fluid Mech.* **210**, 57–112.

Lumley, J. L. 1964 The spectrum of nearly inertial turbulence in a stably stratified fluid. *J. Atmos. Sci.* **21**, 99–102.

Lumley, J. L. 1965 Interpretation of time spectra measured in high-intensity shear flows. *Phys. Fluids* **8**, 1056–1062.

Lumley, J. L. 1967 Similarity and the turbulent energy spectrum. *Phys. Fluids* **10**, 855–858.

Ma, B. & Warhaft, Z. 1986 Some aspects of the thermal mixing layer in grid turbulence. *Phys. Fluids* **29**, 3114–3120.

Makita, H. 1991 Realization of a large-scale turbulence field in a small wind tunnel. *Fluid Dyn. Res.* **8**, 53–64.

Meneveau, C., Sreenivasan, K. R., Kailasnath, P. & Fan, M. S. 1990 Joint multifractal measures: Theory and applications to turbulence. *Phys. Rev.* A **41**, 894–913.

Mestayer, P. G. 1982 Local isotropy and anisotropy in a high-Reynolds-number turbulent boundary layer. *J. Fluid Mech.* **125**, 475–503.

Mestayer, P. G., Gibson, C. H., Coantic M. F. & Patel, A. S. 1976 Local anisotropy in heated and cooled turbulent boundary layers. *Phys. Fluids* **19**, 1279–1287.

Mi, J., Antonia, R. A. & Anselmet, F. 1995 Joint statistics between temperature and its dissipation rate components in a round turbulent jet. *Phys. Fluids* **7**, 1665–1673.

Monin, A. S. & Yaglom, A. M. 1975 *Statistical Fluid Mechanics*, Vol. 2. MIT Press.

Mydlarski, L. & Warhaft, Z. 1996 On the onset of high Reynolds number grid generated wind tunnel turbulence. *J. Fluid Mech.* **320**, 331–368 (referred to herein as M&W96).

Mydlarski, L. & Warhaft, Z. 1998*a* Passive scalar statistics in high-Péclet-number grid turbulence. *J. Fluid Mech.* **358**, 135–175 (referred to herein as M&W98).

Mydlarski, L. & Warhaft, Z. 1998*b* Three-point statistics and the anisotropy of a turbulent passive scalar. *Phys. Fluids* **11**, 2885–2894.

O'brien, E. E. & Jiang, T. 1991 The conditional dissipation rate of an initially binary scalar in homogeneous turbulence. *Phys. Fluids* A **3**, 3121–3123.

Obukhov, A. M. 1949 Structure of the temperature field in turbulent flows. *Izv. Akad. Nauk. SSSR, Geogr. Geofiz.* **13**, 58–69.

Obukhov, A. M. 1962 Some specific features of atmospheric turbulence. *J. Fluid Mech.* **13**, 77–81.

Overholt, M. R. & Pope, S. B. 1996 Direct numerical simulation of a passive scalar with imposed mean gradient in isotropic turbulence. *Phys. Fluids* **8**, 3128–3148 (referred to herein as O&P).

Pope, S. B. 1998 The vanishing effect of molecular diffusivity on turbulent dispersion: implications for turbulent mixing and the scalar flux. *J. Fluid Mech.* **359**, 299–312.

Pope, S. B. 2000 *Turbulent Flows*. Cambridge University Press.

Pope, S. B. & Ching, E. S. C. 1993 Stationary probability density functions: An exact result. *Phys. Fluids* A **5**, 1529–1531.

Prasad, R. R., Meneveau, C. & Sreenivasan, K. R. 1988 Multifractal nature of the dissipation field of passive scalars in fully turbulent flow. *Phys. Rev. Lett.* **61**, 74–77.

Pullin, D. I. 2000 A vortex-based model for the subgrid flux of a passive scalar. *Phys. Fluids* **12**, 2311–2319.

Pumir, A. 1996 Turbulence in homogeneous shear flows. *Phys. Fluids* **8**, 3112–3127.

Pumir, A. & Shraiman, B. I. 1995 Persistent small scale anisotropy in homogeneous shear flows. *Phys. Rev. Lett.* **75**, 3114–3117.

Sabel'nikov, V. A. 1998 Asymptotic solution of the equation for the probability distribution of a passive scalar in grid turbulence with a uniform mean scalar gradient. *Phys. Fluids* **10**, 753–755.

Schmitt, F., Schertzer, D., Lovejoy, S. & Brunet, Y. 1996 Multifractal temperature and flux of temperature variance in fully developed turbulence. *Europhys. Lett.* **34**, 195–200.

She, Z.-S. & Lévêque, E. 1994 Universal scaling laws in fully developed turbulence. *Phys. Rev. Lett.* **72**, 336–339.

Shen, X. & Warhaft, Z. 2000 The anisotropy of the small-scale structure in high-Reynolds-number ($R_\lambda \sim 1000$) turbulent shear flow. *Phys. Fluids* **12**, 2976–2989.

Sinai, Y. G. & Yakhot, V. 1989 Limiting probability distributions of a passive scalar in a random velocity field. *Phys. Rev. Lett.* **63**, 1962–1964.

Sirivat, A. & Warhaft Z. 1983 The effect of a passive cross-stream temperature gradient on the evolution of temperature variance and heat flux in grid turbulence. *J. Fluid Mech.* **128**, 323–346.

Sreenivasan, K. R. 1991 On local isotropy of passive scalars in turbulent shear flows. *Proc. R. Soc. Lond.* A **434**, 165–182.

Sreenivasan, K. R. & Antonia, R. A. 1977 Skewness of temperature derivatives in turbulent shear flows. *Phys. Fluids* **20**, 1986–1988.

Sreenivasan, K. R. & Antonia, R. A. 1997 The phenomenology of small-scale turbulence. *Annu. Rev. Fluid Mech.* **29**, 435–472.

Sreenivasan, K. R., Antonia, R. A. & Danh, H. Q. 1977 Temperature dissipation fluctuations in a turbulent boundary layer. *Phys. Fluids* **20**, 1238–1249.

Sreenivasan, K. R. & Kailasnath, P. 1993 An update on the intermittency exponent in turbulence. *Phys. Fluids* **5**, 512–514.

Tavoularis, S. & Corrsin, S. 1981 Experiments in nearly homogeneous turbulent shear flow with a uniform mean temperature gradient. Part 1. *J. Fluid Mech.* **104**, 311–347.

Taylor, G. I. 1921 Diffusion by continuous movements. *Proc. Lond. Math. Soc.* **20**, 196–212.

Taylor, G. I. 1938 The spectrum of turbulence. *Proc. R. Soc. Lond.* A **164**, 476–490.

Tennekes, H. & Lumley, J. L. 1972 *A First Course in Turbulence.* MIT Press.

Thoroddsen, S. T. & Van Atta, C. W. 1992 Exponential tails and skewness of density-gradient probability density functions in stably stratified turbulence. *J. Fluid Mech.* **244**, 547–566.

Tong, C. & Warhaft, Z. 1994 On passive scalar derivative statistics in grid turbulence. *Phys. Fluids* **6**, 2165–2176.

Townsend, A. A. 1976 *The Structure of Turbulent Shear Flows.* Cambridge University Press.

Van Atta, C. W. 1974 Influence of fluctuations in dissipation rates on some statistical properties of turbulent scalar fields. *Izv. Atmos. Ocean. Phys.* **10**, 712–719.

Venkataramani, K. S. & Chevray, R. 1978 Statistical features of heat transfer in grid-generated turbulence: constant-gradient case. *J. Fluid Mech.* **86**, 513–543.

Wang, L., Chen, S. & Brasseur, J. G. 1999 Examination of hypotheses in the Kolmogorov refined turbulence theory through high-resolution simulations. Part 2. Passive scalar field. *J. Fluid Mech.* **400**, 163–197.

Warhaft, Z. & Lumley, J. L. 1978 An experimental study of the decay of temperature fluctuations in grid generated turbulence. *J. Fluid Mech.* **88**, 659–684.

Warhaft, Z. & Shen, X. 2001 Some comments on the small-scale structure of turbulence at high Reynolds number. *Phys. Fluids* **13**, 1532–1533.

Wyngaard, J. C. 1971 The effect of velocity sensitivity on temperature derivative statistics in isotropic turbulence. *J. Fluid Mech.* **48**, 763–769.

Xu, G., Antonia, R. A. & Rajagopalan, S. 2000*a* Scaling of mixed longitudinal velocity-temperature structure functions. *Europhys. Lett.* **49**, 452–458.

Xu, G., Antonia, R. A. & Rajagopalan, S. 2000*b* Scaling of mean temperature dissipation rate. *Phys. Fluids* **12**, 3090–3092.

Yaglom, A. M. 1949 On the local structure of a temperature field in a turbulent flow. *Dokl. Akad. Nauk. SSSR* **69**, 743–746.

Yoon, K. & Warhaft, Z. 1990 The evolution of grid-generated turbulence under conditions of stable thermal stratification. *J. Fluid Mech.* **215**, 601–638.

Zhou, T., Antonia, R. A., Danaila, L. & Anselmet, F. 2000 Transport equations for the mean energy and temperature dissipation rates in grid turbulence. *Exps. Fluids* **28**, 143–151.

Zhu, Y., Antonia, R. A. & Hosokawa, I. 1995 Refined similarity hypotheses for turbulent velocity and temperature fields. *Phys. Fluids* **7**, 1637–1648.